ANALISIS DE INTERFEROGRAMAS CON PORTADORAS ESPACIALES LINEAL Y RADIAL

Presentada por Jorge Luis García Márquez
Como un requisito parcial para optar por el grado
Doctor en Ciencias (Optica)

Bajo la supervisión del profesor Daniel Malacara Hernández
Grupo de Interferometría

El Centro de Investigaciones en Optica A.C.
y la Universidad de Guanajuato

LINEAR AND RADIAL SPATIAL CARRIER ANALYSIS OF INTERFEROGRAMS

Presented by Jorge García-Márquez
Submitted in Partial Fulfillment of the Requirements for the Degree
Doctor of Philosophy

Academic adviser: Professor Daniel Malacara-Hernández
Group of Interferometry

The Centro de Investigaciones en Optica A.C.
and the Universidad de Guanajuato
León, México, November 1998

Contents

Preface 1

Prefacio 3

Chapter I. ***General Review of Fringe Analysis Methods*** 5

1.1 Introduction 6

1.1.1 Single Pattern Analysis 7

1.1.2 Multiple Pattern Analysis 8

1.2 Frequency Domain 12

1.2.1 Method Proposed by Takeda *et al* 12

1.2.2 Method Proposed by Kreis 14

1.3 Space Domain 15

1.3.1 Method Proposed by Womack 15

1.3.2 Method Proposed by Moore 16

1.4 References 19

Chapter II. ***Analysis of Interferograms with a Spatial Radial and Linear Carrier*** 32

2.1 Introduction 33

2.2 Interferograms with a Radial or Circular Carrier 34

2.3 Phase Demodulation of Closed Fringe Patterns 36

2.3.1 Phase Demodulation with a Radial Reference Carrier (Spherical Reference Wavefront) 36

2.3.2 Phase Demodulation with a Linear Reference Wavefront (Tilted Plane Reference Wavefront) 40

2.4 The Method Proposed by García-Márquez *et al.* A Review 44
2.5 Analysis of Error and its Sources 44
2.5.1 RMS and Maximum Error with a Square Filter 44
2.5.2 Recursive Method for Radial Reference Carrier Demodulation 45
2.6 References 48

Chapter III. *Holographic and Moiré Aspherical Compensators* 69
3.1 Introduction 70
3.2 Theory 71
3.3 Holographic and Moiré Compensators 74
3.3.1 Hologram Inside the Interferometer Cavity 74
3.3.2 Hologram Outside the Interferometer Cavity 75
3.3.3 Hologram in Front of the Interferometer Cavity 75
3.4 Demodulating an Interferogram with a Linear Carrier 76
3.5 References 78

Conclusions 85
Conclusiones 87

Acknowledgments

I wish to acknowledge the Consejo Nacional de Ciencia y Tecnología and the Dirección de Formación Académica from the Centro de Investigaciones en Optica A.C. for his financial support.

To my wife

To my parents and brothers

To my colleagues

Preface

The importance of aspheres is growing up every day, it can be seen in different fields, from ophthalmology to astronomy, in the laboratory and in fiber optic communications. It is well known that the quality in optical manufacturing depends on the accuracy of the method used to test. The aim of this thesis is to test aspheric wavefronts in a simple way. It means without the intrinsic restrictions of introducing a linear carrier frequency (e.g by tilting a reference surface) nor those when taking several frames (Phase Shifting Interferometry). The importance of the analysis of interferograms with the introduction of a reference carrier frequency will be explained here with some detail.

In chapter one an introduction to the main techniques on single pattern analysis is made. A comparison between a single pattern analysis and multiple pattern analysis techniques is also done.

It is well known that an interferogram can be demodulated to find the wavefront shape if a linear carrier is introduced. In chapter two it is shown that the interferogram can also be demodulated if it has many closed fringes or a circular carrier appear. The demodulation is made in the space domain, as opposed to demodulation in the Fourier space, but the low pass filter characteristics must be properly chosen. For academic purposes an holographic analogy of this demodulation process is also presented, which shows that the common technique of multiplying by a sine and a cosine function is equivalent to holographically reconstructing with a flat tilted wavefront. Alternatively, a defocused (spherical) wavefront can be used as a reference to perform the reconstruction or demodulation of some closed fringe interferograms. In addition to this, an analysis of the Root Mean Square Error (RMS error) is presented and an algorithm to reduce this error in the phase demodulation process is proposed. It should be pointed out that when commercial

interferometers tests optical surfaces, they need no more than five fringes in order to have a quite good resolution. It means that if the measuring field has 256 pixels in both x and y directions, each fringe covers more than 50 pixels. More over, Phase Shifting Interferometry require the existence of a small number of fringes over the field in order to have a good set of acquisition frames. In the method proposed here it does not matter whether a large fringe frequency appears at the edges of an interferogram with aspherical aberration.

Incidentally, computer generated aspherical compensators are superimposed on an interferometer wavefront or fringe pattern to obtain a null fringe pattern. This process has been understood and widely described in the literature. On the other hand, when we superimpose an ideal fringe pattern on top of the picture of an interferogram to be analyzed, we obtain a moiré pattern between the two images. These two apparently different procedures have much in common, but also some important differences to be described in chapter three. Furthermore a Ronchi ruling can be used to remove the linear frequency in the interferogram instead of an holographic process, this process is known as interferogram demodulation with a linear carrier.

Prefacio

Hoy en día la importancia de las asferas crece rápidamente, esto se puede constatar en campos tan diferentes que van de la oftalmología a la astronomía, en el laboratorio o en las comunicaciones con fibra óptica. Por otro lado, se sabe que para poder obtener buenas calidades en un taller de fabricación óptica es necesario un muy buen método de prueba. El propósito de esta tesis es probar frentes de onda asféricos de una manera más sencilla, esto es, sin las restricciones intrinsecas de la frecuencia portadora lineal ni aquellas de la interferometría de desplazamiento de fase. La importancia del análisis de interferogramas con la introducción de una frecuencia portadora de referencia será explicada a detalle.

El capítulo uno es dedicado a una introducción al estudio de las principales técnicas de análisis de interferogramas reportadas en las revistas científicas. Así mismo se hace una comparación entre las técnicas de análisis de patrones de franjas en base a una toma y a múltiples tomas.

Por otro lado, es bien sabido que para recuperar la forma de un frente de onda, se debe introducir una portadora lineal en el interferograma. En esta tesis, se demuestra que si el interferograma carece de portadora lineal, pero tiene una portadora radial (franjas circulares) puede ser también demodulado. Esta demodulación se realiza en el dominio espacial, caso contrario a aquella en el dominio de las frecuencias (Fourier), sin embargo las características que debe llevar el filtro pasa bajas deben ser propiamente seleccionadas. Por razones académicas se presenta una analogía holográfica a este proceso de demodulación, la cual muestra que las técnicas comunes de demodulación, a partir de la multiplicación del

interferograma por una función seno y otra coseno, es equivalente a reconstruir un holograma con un frente plano inclinado. Una alternativa es utilizar un frente de onda esférico (desenfocado) como frente de reconstrucción (demodulación) para algunos interferogramas de franjas cerradas. Para el método propuesto, es también presentado un análisis de error cuadrático medio y proponemos un algoritmo para reducir este error. Debemos señalar que cuando se realizan pruebas ópticas con interferómetros comerciales, se hace necesario tener un patrón de franjas no mayor de cinco franjas para todo el campo. Esto significa que si el campo es de 256 pixeles en cada eje, cada franja ocupa alrededor de 50 pixeles. Por otro lado, la Interferometría de Desplazamiento de Fase (análisis con múltiples patrones) requiere la existencia de no muchas franjas a fin de aumentar su precisión. En la técnica presentada en esta disertación, deseamos no exceder el límite de Nyquist, esto es, se pueden resolver interferogramas con una gran cantidad de franjas. Así, al probar un frente de onda asférico, no importa mucho la gran frecuencia espacial en el borde del interferograma.

Por otro lado, un compensador asférico generado por computadora es superpuesto en el patrón de franjas de un interferómetro, a fin de generar un patrón de franjas nulo. Este proceso ya ha sido reportado ampliamente en la literatura. Mas aún, cuando se superpone un patrón de franjas ideal sobre el negativo de un interferograma, se obtiene un patrón de franjas de moiré de estas dos imagenes. Aparentemente, estos dos métodos son muy similares, sin embargo, tienen diferencias que son importantes y que serán descritas en este capítulo.

Chapter I

General Review of Fringe Patterns Analysis Methods

1.1 INTRODUCTION

There are several coherent optical interferometry techniques that encode phase information coming on from a distorted object, in the form of interference fringes. A large number of techniques used to extract the phase information from these objects has been investigated and reported in the literature [1,2]. These techniques are known as fringe analysis methods and can be divided in the following manner:

I.- Single fringe pattern analysis

a) Fringe sampling with global and local interpolation: Direct calculations, fringe tracking, global polynomial interpolation, local interpolation by segments.

b) Space heterodyne demodulation of fringe pattern (direct-measuring interferometry): Spatially phase-stepped, carrier frequency, spatial synchronous detection (direct interferometry), phase locked loop.

c) Fourier analysis of fringe patterns: Fourier transform

II. Multiple fringe pattern analysis

d) Phase-shifting methods (temporal domain): phase shifting, heterodyne, phase-lock.

The advantages and disadvantages of single and multiple pattern analysis are:

1. While in multiple pattern analysis methods a minimum of three interferogram frames are needed, in single pattern analysis methods only one is necessary.

2. The multiple pattern methods require an accurately calibrated phase shifter device (i.e. a piezoelectric transducer, a rotating glass plate, a moving diffraction grating). In single pattern methods a really sophisticated mathematical analysis or computational processing is needed.

3. In multiple pattern methods three or more frames must be taken simultaneously in order to avoid the effect of vibrations. In single pattern methods there is no problem, since only one frame is taken. In addition to this, in mechanics the study of transient deformations requires that the phase be extracted from a single interferogram. It is possible some times to have an environment free of vibrations or turbulence (e.g. deflectometry) and multiple pattern methods are more accurate and have more precision.

4. In multiple pattern methods the sign of the wavefront deformation is determined. In single pattern methods an aberration with a known sign should be introduced in order to determine the sign of the wavefront.

1.1.1 Single Pattern Analysis

This section includes several and interesting manners to retrieve the phase from an interferogram.

The group of methods involving the fringe sampling with global and local interpolation, uses sophisticated numerical analysis to process the interferogram as an ordinary image. If we have two interfering wavefronts, one of them plane and acting as a reference, the other one also plane but tilted and coming on as the object wavefront, we will have a system of straight, parallel and equidistant fringes. When the wavefront under test is not flat, the fringes do not appears straight but curved. These fringes are called equal-thickness fringes because they represent the locus of the points with constant wavefront separation. In this manner, the deformations on the object may be estimated from a visual examination of their deviation from straightness in the interferogram. Some systems had been developed to perform semi-automatic analysis of fixed interferograms[3] and reviews of their implicit problems have been published [4,5].

The fringes can be located by manually marking its center (using a digitizing tablet) or automatically, making the mark directly over a frame fringe pattern, previously captured

using a digital frame grabber. After locating all the fringe centers, fringe order numbers must be assigned to each point. Then, either the interferogram fringe centers can be characterized by direct analysis of the ordered fringe center, or it can be used to generate a uniform grid of data representing a map of the wavefront optical path difference (OPD).

In the first case the analysis results take the form of wavefront statistics, such as peak-to-valley (PV) and root-mean-square (RMS) wavefront error. Reducing all measured wavefronts to a uniform data grid it is possible to graphically display the optical phase difference as a phase map, and perform some analysis such as diffraction patterns. Because the fringe centers represents de phase map measurements at discrete points, the data interpolation between the fringes will be required to produce the uniform grid.

The two methods used more often to estimate the complete wavefront shape are global polynomial fitting and local interpolation using splines. In global interpolation, a single analytical two-dimensional function is used to represent the wavefront for the whole interferogram. To perform a global interpolation the polynomials most frequently used are the Zernike polynomials [6].

The second and third kind of methods that we will treat in subsections 1.2 and 1.3 are also called spatial carrier fringe pattern analysis. Both of them use the holographic theory of phase modulation and demodulation, implement the entire demodulation procedure in a computer image processing and yield in a direct way the two-dimensional phase distribution wich modulated the spatial reference carrier.

1.1.2 Multiple Pattern Analysis

Finally, phase shifting Interferometry methods (PSI) are another group of fringe pattern analysis methods. PSI electronically records a series of interferograms while the reference phase of the interferometer is changed. The wavefront phase is modulated in the variations in the intensity pattern of the framed interferograms, and the phase is recovered by a point-by-point calculation. There is no need to locate the fringe centers. Up to now

many relevant works have been published in this field [7,8,9,10] and have been extended to speckle pattern interferometry. In phase shifting interferometry the reference wavefront is moved along the direction of propagation, with respect to the object wavefront changing their phase difference. By measuring the irradiance change for different phase shifts, it is possible to determine the phase for the object wavefront, relative to the reference wavefront, for the measured point on the wavefront. All electric devices do not measure amplitude but irradiance and irradiance signal $I(x,y)$ at the point (x,y) in the detector changes with the phase, as

$$s(x,\ y,\ \alpha) = a + b\ \cos\ [\phi(x,\ y) + \alpha] \tag{1.1}$$

where $\phi(x,y)$ is the phase at the origin and α is a known phase shift with respect to the origin, a is the background intensity and b is the modulation amplitude of the fringes, directly proportional to the visibility. From equation 1.1 there are three unknowns and only one equation, then we need at least another two different frames with a shifted phase α to determine the complete wavefront shape.

Incidentally, there are some analysis methods used in PSI techniques. Greivenkamp [11] has developed a diagonal least squares algorithm whereby the phase is extracted by means of equally and uniformly spaced sampling points,

$$\tan\phi(x,y) = -\left(\frac{\sum_{n=1}^{N} s_n \sin\left(\frac{2\pi n}{N}\right)}{\sum_{n=1}^{N} s_n \cos\left(\frac{2\pi n}{N}\right)} \right) . \tag{1.2}$$

Here, the minimum acceptable number of sampling points is N=3.

As a generalization, the study of the synchronous detection from a Fourier point of view was later developed by Freischlad and Koliopoulos [12]. They removed the restrictions of equally and uniformly spaced sampling points. Thus their theory shows that the phase ϕ is in general given by,

$$\tan\phi(x,y) = -\frac{\int_{-\infty}^{\infty} s(x)g_1(x)dx}{\int_{-\infty}^{\infty} s(x)g_2(x)dx}. \tag{1.3}$$

As long as four conditions to be described below are satisfied. Two general assumptions must be taken into account:

1. The signal to be detected is periodic but not necessarily sinusoidal, it means that it may contain harmonics.
2. The two general functions $g_1(x)$ and $g_2(x)$ are used in lieu of the sine and cosine functions.

This method requires that

1. The Fourier elements of the reference functions $g_1(x)$ and $g_2(x)$ must have a zero DC term. Then its Fourier transforms $G_1(f)$ and $G_2(f)$ at zero frequency also must be equal to zero.
2. All interference between undesired harmonics in the signal and in the reference functions must be avoided.
3. The Fourier elements of the reference functions $g_1(x)$ and $g_2(x)$ at the frecuency f_r must be orthogonal to each other. This means that the Fourier transforms $G_1(f)$ and $G_2(f)$ of these two reference functions at the frequency f must have a phase difference equal to $\pm\pi/2$.
4. The Fourier transforms $G_1(f)$ and $G_2(f)$ of these two reference functions, at the

frequency f_r must have the same magnitude.

If the sampling functions $g_1(x)$ and $g_2(x)$ are discrete (discrete sampling instead of continous) and these four conditions are applied, the value of the phase ϕ may be calculated by

$$\phi(x,y) = \mp \tan^{-1}\left(\frac{\sum_{n=1}^{N} s(x_n)W_{1n}}{\sum_{n=1}^{N} s(x_n)W_{2n}}\right) . \qquad (1.4)$$

where W_{in} is the sampling weight for sampling point i and N is the number of sampling points with coordinates $x = x_n$.

An alternative way to express the phase ϕ is by saying that this is the phase of the complex function $V(\phi)$,

$$V(\phi) = \sum_{n=1}^{N}\left(W_{1n} + iW_{2n}\right) s(x_n) \qquad (1.5)$$

This function $V(\phi)$ is known as the characteristic polynomial, proposed by Surrel [13]. This polynomial may be used to derive all main properties of the algorithm, in a form closely associated with the Fourier theory for the Freischlad and Koliopoulos' case. After several manipulations this polynomial may be expresed as a function of the harmonics (z) as follows

$$P(z) = \sum_{n=1}^{N}\left(W_{1n} + iW_{2n}\right)\left(e^{im\Delta\alpha}\right)^{(n-1)} \qquad (1.6)$$

where α_n is the phase for the sampling point n, $\Delta\alpha$ is the phase interval separation between the sampling points and z is associated to a harmonic number m, by $z = e^{im\Delta\alpha}$. These values of z may be represented in a unit circle in the complex plane. Given a sampling algorithm, the value of the phase interval $\Delta\alpha$ between sampling points is fixed, i.e. there is a point for each possible value of the harmonic number, including positive as well as negative numbers. Here

we refer the readers to the original article to see the characteristic diagram of the sampling algorithms and its properties.

1.2 FREQUENCY DOMAIN

As we have seen in the previous section, in multiple pattern analysis several frames have to be measured. This requires the shifting of the phase by means of, for example, a piezoelectric crystal. In frequency and spatial domain single pattern methods described in these two following sections, only a single frame is necessary to obtain the wavefront.

1.2.1 The Method Proposed by Takeda *et al*

In single pattern analysis it is possible to study the interferogram in the space domain [14] (interferogram plane) or in the frequency domain [15] (Fourier plane).

Consider a digitized fringe pattern where the intensity at each point in the image, $s(x,y)$, is described by

$$s(x, y) = a(x,y) + b(x,y) \cos [\phi(x, y) + 2\pi f_0 x] \tag{1.7}$$

where $\phi(x,y)$ is the phase of the object and $a(x,y)$, $b(x,y)$ and $\phi(x,y)$ are assumed to vary slowly compared with a spatial carrier frequency, f_0, introduced into the interferometer. Equation (1.7) can be rewritten as:

$$s(x, y) = a(x,y) + c(x,y)\, e^{i2\pi f_0 x} + c^*(x,y)\, e^{-i2\pi f_0 x} \tag{1.8}$$

where

$$c(x, y) = \frac{1}{2} b(x,y)\, e^{i\phi(x,y)} \tag{1.9}$$

and an asterisk denotes a complex conjugate. Equation (1.8) is then Fourier transformed with

respect to the x-axis by a fast Fourier transform (FFT) algorithm,

$$\mathcal{F}[s(x, y)] = \mathcal{F}[a(x,y)] + \int_{-\infty}^{\infty} c(x,y)\, e^{i2\pi f_0 x} e^{-i2\pi f x}\, dx + \int_{-\infty}^{\infty} c^*(x,y)\, e^{-i2\pi f_0 x} e^{-i2\pi f x}\, dx \tag{1.10}$$

This gives:

$$S(f, y) = A(f,y) + C(f-f_0,y) + C^*(-f-f_0,y) \tag{1.11}$$

the capital letter denotes the Fourier transform and f is the spatial frequency in the x direction. Fig. 1.1(a) shows the intensity distribution of equation 1.7 and in Fig. 1.1(b) is its Fourier spectral frequency in the x direction. A carrier frequency, $f_0 = 40$ fringes/field (field = 256) is used. A filter $H(x,,y)$, is used to isolate one of the two sidebands or lobes, for example $C(f-f_0,y)$ in Fig. 1.1(b). After this lobe is shifted by$_0 f$ towards the origin on the frequency axis to obtain $C(f,y)$ as is shown in Fig. 1.1(c). Considering the filter applied to the shifted frequency spectrum, we can write:

$$C(f, y) = H(f,y)\ S(f+f_0,y) \tag{1.12}$$

The unwanted background intensity $a(x,y)$ has been filtered out at this moment. The spectrum of equation (1.12) is shifted back to the frequency plane origin, prior to performing an inverse transform (again with the FFT). The result of the Fourier transform gives $c(x,y)$, eqn (1.9), and the wavefront phase can be recovered from this using,

$$\phi(x,y) = \tan^{-1} \frac{Im[c(x,y)]}{Re[c(x,y)]} \tag{1.13}$$

The arctan function calculates the arctangent over a full -π to π range. The phase given by this equation is modulo 2π and is sometimes referred to as a *wrapped phase*[15]. The *unwrapped*, or true, phase is obtained by removing the discontinuities that occur when the phase suddenly jumps from -π to π. Whe the unwrapped phase is gotten, the analysis of

interferograms in the frequency domain is completed. Finally, if the Fourier spectra sideband (lobe) $C(f-f_0,y)$ is not shifted in frequency to the origin then the inverse Fourier transform is given by $c(x,y)e^{i2\pi f_0 x}$, and the phase calculated from eqn (1.13) is $\phi(x,y) + 2\pi f_0 x$, it means that it still contains the carrier frequency.

1.2.2 The Method Proposed by Kreis

Kreis [16] proposed that the Fourier transform method could be used without a spatial carrier frequency. From Eqn (1.7) $f_0 = 0$ and it can be rewritten as

$$s(x, y) = a(x,y) + c(x,y) + c^*(x,y) \tag{1.14}$$

where $c(x,y)$ is defined by eqn. (1.9). This procedure is illustrated in Fig. 1.2, for the same phase distribution as Fig. 1. Next Eqn. (1.14) is Fourier transformed, which may be done one-dimensionally with respect to x, giving

$$S(f, y) = A(f,y) + C(f,y) + C^*(f,y) \tag{1.15}$$

In general the Fourier spectra are not now separated, Fig. 1.2(b). A band-pass filter is applied in Fig. 1.2(c); notice that the filtered out Fourier spectrum does not need to be shifted and that blocking either positive or negative frequencies means that the calculated phase distribution can only increase or decrease in the x direction. Thus, a phase inversion takes place for non-monotonic phase distributions. Nevertheless, this ambiguity can be solved using two fringe patterns, recorded with a known phase displacement α between them,

$$\begin{aligned} s_1(x, y, \alpha) &= a + b \cos [\phi(x, y)] \\ s_2(x, y, \alpha) &= a + b \cos [\phi(x, y) + \alpha] \end{aligned} \tag{1.16}$$

where $\alpha < \pi$ rad. The phase calculated by eqn (1.13) is multiplied by the calculated sign of α at each point to resolve the direction of displacement. In spite of having not one but two fringe patterns, it is not necessary to know or to control the exact phase shift. However, only the sign of α is of interest.

1.3 SPACE DOMAIN

Spatial domain single pattern analysis is considerably faster than frequency domain methods, and could enable phase to be calculated in real time on a modest personal computer.

1.3.1 The Method Proposed by Womack

The first work on space domain processing has been reported by using an analogue circuit by Ichioka and Inuiya [17]. Later Womack[14] was concerned on the same topic. Assuming again eqn. (1.7) and multiplying it by a frequency f_0,

$$s(x, y) = \left[a(x,y) + b(x,y) \cos\left[\phi(x, y) + 2\pi f_0 x\right]\right] e^{i2\pi f_0 x} \tag{1.17}$$

this yields to the following expressions:

$$s(x, y) \sin(2\pi f_0 x) = a(x,y) \sin(2\pi f_0 x) + \frac{1}{2} b(x,y) \sin[\phi(x, y) + 4\pi f_0 x] \\ \frac{1}{2} b(x,y) \sin[\phi(x, y)] \tag{1.18a}$$

and

$$s(x, y) \cos(2\pi f_0 x) = a(x,y) \sin(2\pi f_0 x) + \frac{1}{2} b(x,y) \cos[\phi(x, y) + 4\pi f_0 x] \\ \frac{1}{2} b(x,y) \cos[\phi(x, y)] \tag{1.18b}$$

or in an analogous manner

$$Z_s = s(x, y)\ \sin(2\pi f_0 x) \tag{1.19a}$$

and

$$Z_c = s(x, y)\ \cos(2\pi f_0 x) \tag{1.19b}$$

Figure 1.3(a) shows a fringe pattern identical to that in Fig. 1.1(a) *i.e.* $f_0 = 40$ fringes/field (field = 256), giving a carrier wavelength of $\lambda_0 = \text{field}/f_0 = 6.4$ pixels. Figure 1.3(b) shows the pattern correspondent to eqn (1.19b). To have an idea of Fourier plane behavior, the images in the frequency domain are shown. As we will notice from eqn (1.18b) the only term centered about the frequency origin is the third. Thus this term can be isolated by the application of a low-pass average filter (Fig. 1.3(c)) equal to the carrier-fringe wavelength, λ_0,

$$h(x,y) = rect\left(\frac{x}{\lambda_0}\right) \tag{1.20}$$

the response in the frequency domain is given by

$$H(x,y) = sinc(\pi f \lambda_0) \tag{1.21}$$

Finally the phase can be calculated by:

$$\phi(x,y) = \tan^{-1}\left[-\frac{h(x,y) * Z_s}{h(x,y) * Z_c}\right] \tag{1.22}$$

where an asterisk denotes convolution.

1.3.1 The Method Proposed Moore

Moore and Mendoza-Santoyo [18] were concerned on a space domain method without

carrier. Their work is related with that of Kreis [16] but the analysis is made in the interferogram plane. From eqn (1.7) with $f_0 = 0$,

$$s(x, y)\ \sin(2\pi f_0 x) = a(x,y)\ \sin(2\pi f_0 x) + \frac{1}{2}b(x,y)\ \sin[\phi(x, y) + 2\pi f_0 x] - \frac{1}{2}b(x,y)\ \sin[\phi(x, y) - 2\pi f_0 x] \quad (1.23a)$$

and

$$s(x, y)\ \cos(2\pi f_0 x) = a(x,y)\ \cos(2\pi f_0 x) + \frac{1}{2}b(x,y)\ \cos[\phi(x, y) + 2\pi f_0 x] - \frac{1}{2}b(x,y)\ \cos[\phi(x, y) - 2\pi f_0 x] \quad (1.23b)$$

or equivalently

$$Z_s = s(x, y)\ \sin(2\pi f_0 x) \quad (1.24a)$$

and

$$Z_c = s(x, y)\ \cos(2\pi f_0 x)\ . \quad (1.24b)$$

Figure 1.4(a) shows the intensity profile along the x direction of the phase distribution of f = 6.4 fringes/field. This is then multiplied by a linear carrier of $\cos(2\pi f_0 x)$, Fig. 1.4(b), where f_0 = 40 fr/fd (λ = field/f = 6.4 pixels). Although the choose of carrier is completly arbitrarily. Then a low-pass filter is applied to the image to isolate the third term in eqn. 1.23(b). Obviously the three terms of the spectra are centered about the axis in the frequency domain. A low-pass filter of size λ_0 is applied (Fig. 1.4(c)), and the phase calculated from:

$$\phi(x,y) - 2\pi f_0 x = \tan^{-1}\left[-\frac{h(x,y) * Z_s}{h(x,y) * Z_c}\right] \tag{1.25}$$

As we can notice the carrier frequency used in the demodulation process is still contained in the result Fig. 1.4(d), and should be substracted it out, Fig. 1.4(e). As in other techniques that use a single pattern without carrier, this one also has an indetermination on the sign of ϕ. Thus the real sign of the phase must be determined from knowledge of object loading conditions. Moore [18] has shown that in order to have a good accuracy by using this method, the reference linear carrier must closely match the frequency of the interferogram.

1.4 REFERENCES

[1] Malacara, D., Optical Shop Testing, John Wiley, second ed., New York (1992).

[2] Vlad, V. I. and D. Malacara, "Direct spatial reconstruction of optical phase from phase-modulated images," in *Progress in Optics,* Vol. XXXIII, E. Wolf ed.,Elsevier, North-Holland, Amsterdam, 261-317 (1994).

[3] Womack, K. H., J. A. Jonas, C. L. Koliopoulos, K. L. Underwood, J. C. Wyant, J. S. Loomis and C. R. Hayslett, "Microprocessor-based instrument for analysis of video interferograms," *Proc. SPIE*, **192**, 134-139 (1979).

[4] Reid, G. T., "Automatic fringe pattern analysis: a review," *Opt. And Lasers in Eng.*, **7**, 37-68 (1986/87).

[5] Reid, G. T., "Image processing techniques for fringe pattern analysis," *Proc. SPIE*, **954**, 468-477 (1988).

[6] Malacara, D., J. M. Carpio and J. Sánchez-Mondragón, "Wavefront fitting with discrete orthogonal polynomials in a unit radius circle," *Opt. Eng.*, **29**, 672-675 (1990).

[7] Carré, P., "Installation et utilization du comparateur photoelectrique et interferentiel du bureau international des poids et measures," *Metrologia*, **2**, 13-23 (1966).

[8] Bruning, J. H., D. R. Herriot, J. E. Gallagher, D. P. Rosenfeld, A. D. White and D. J. Brangaccio, "Digital wavefront measuring interferometer for testing surfaces and lenses," *Appl. Opt.*, **13**, 2693-2703 (1974).

[9] Greivenkamp, J. E. and J. H. Bruning, "Phase shifting interferometry," in *Optical Shop Testing*, 2nd Edition, D. Malacara, Ed., John Wiley and Sons, New York, 1992.

[10] Schwider, J., "Advanced evaluation techniques in interferometry," in *Progress in Optics*, **XXVIII**, E. Wolf, Ed. Elsevier North-Holland, Amsterdam, 1990.

[11] Greivenkamp, J.E., "Generalized data reduction for heterodyne interferometry," *Opt. Eng.*, **23**, 350-352 (1984).

[12] Freischlad, K. and C. L. Koliopoulos, "Fourier description of digital phase measuring interferometry," *J. Opt. Soc. Am. A*, 7, 542-551 (1990).

[13] Surrel, Y., "Design os algorithms for phase measurements by the use of phase stepping," *Appl. Opt.*, **35**, 51-60 (1996).

[14] Womack, K. H., "Interferometric phase measurement using spatial synchronous detection," *Opt. Eng.*, **23**, 391 (1984).

[15] Takeda, M., I. Hideki and S. Kobayashi, "Fourier-transform method of fringe pattern analysis for computer based topography and interferometry," *J. Opt. Soc. Am.*, **72**, 156 (1982).

[16] Kreis, T., "Digital holographic interference-phase measurement using the Fourier-transform method," *J. Opt. Soc. Am. A*, **3**, 847 (1986).

[17] Ichioka, Y. and M. Inuiya, "Direct phase detecting systems," *Appl. Opt.*, **11**, 1507 (1998).

[18] Moore, A. J. and F. Mendoza-Santoyo, "Phase demodulation in the space domain without a fringe carrier," *Opt. Las. Eng.*, **23**, 319 (1995).

[19] Servín, M., J. L. Marroquín and F. J. Cuevas, "Demodulation of a single interferogram by use of a two-dimensional regularized phase-tracking technique," *Appl. Opt.*, **36**, 4540 (1997).

[20] García-Márquez, J., D. Malacara-Hernández and M. Servín, "Holographic analogy of the spatial radial carrier analysis of interferograms," *Proc. SPIE*, **2860**, 394 (1996).

Figure Captions

Figure 1.1.- Fourier transform method with fringe carrier, (a) $\phi(x,y)$, (b) its Fourier transform, (c) $\phi(x,y) + 2\pi f_0 x$ (d) Fourier transform and filter, (e) shifted spectra, (f) unwrapped phase.

Figure 1.2.- Fourier transform method without fringe carrier, (a) intensity distribution (x,y), (b) its Fourier transform, (c) filter spectra, (d) unwrapped phase.

Figure 1.3.- Spatial Synchronous detection with fringe carrier, (a) intensity distribution $\phi(x,y)$, (b) its Fourier transform, (c) $\phi(x,y) + 2\pi f_0 x$ (d) its Fourier transform, (e)intensity distribution multiplied by carrier frequency, (f) its Fourier transform, (g) low-pass filter applied to (c), (h) Fourier transform, (i) unwrapped phase.

Figure 1.4.- Spatial Synchronous detection without fringe carrier, (a) intensity distribution $\phi(x,y)$, (b) its Fourier transform, (c) intensity distribution multiplied by carrier frequency $\phi(x,y) + 2\pi f_0 x$ (d) its Fourier transform,(e) low-pass filter applied to (c), (f) Fourier transform, (g) unwrapped phase.

(a.u.)

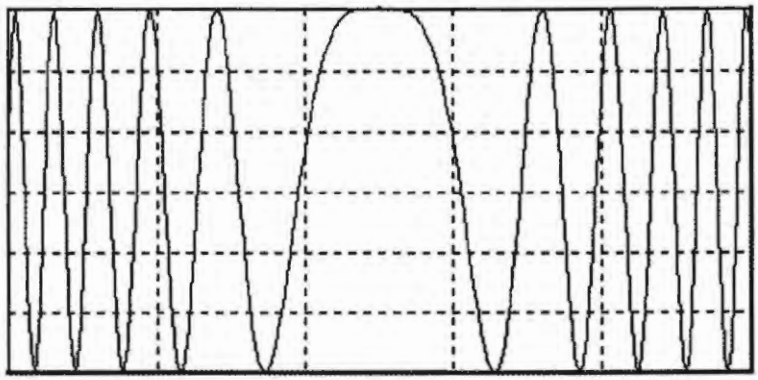

(a)

(a.u.)

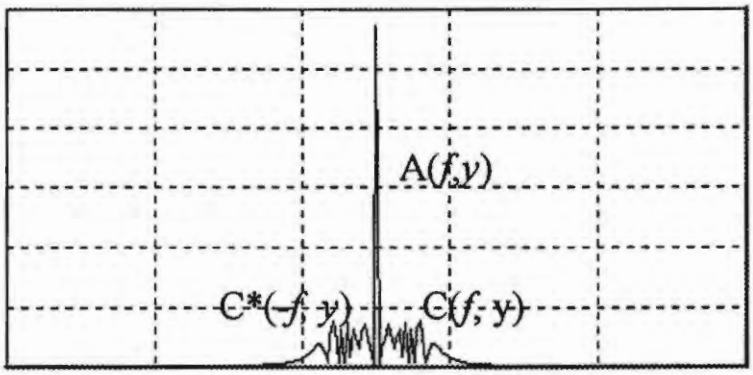

(b)

(a.u.)

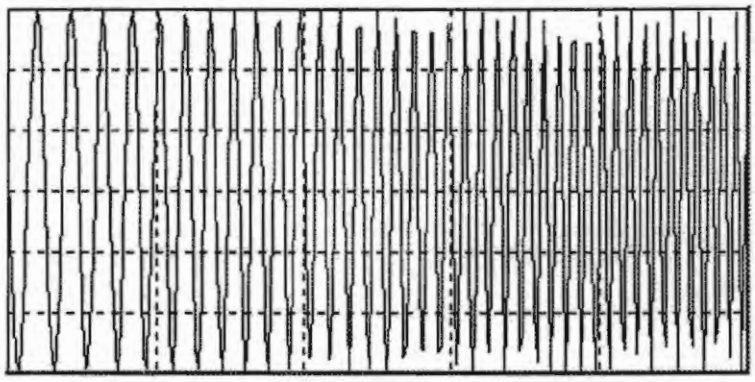

(c)

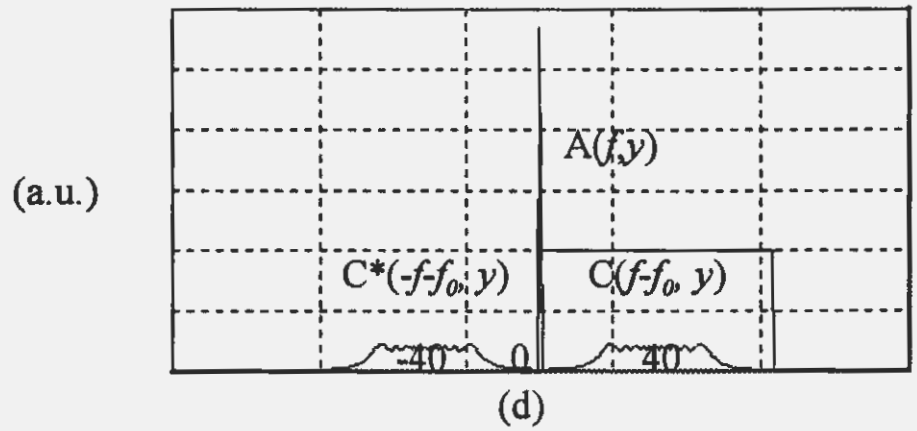

(d)

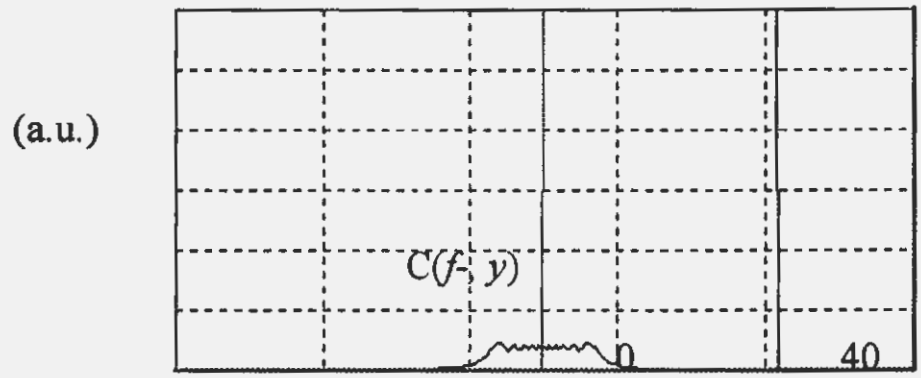

(e)

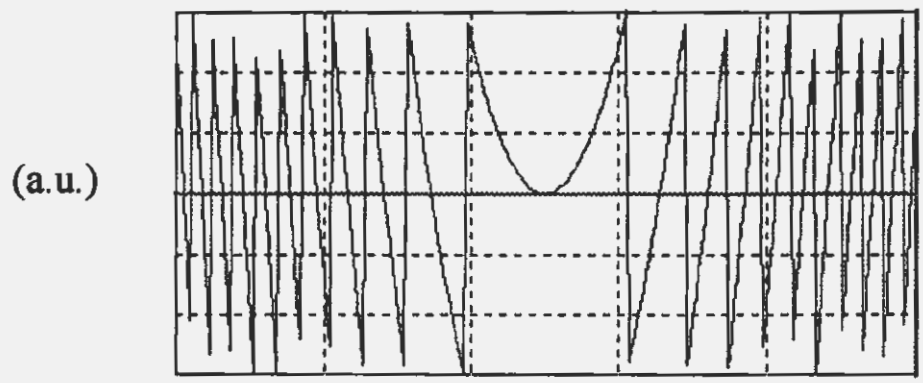

(f)

Figure 1.1

(a.u.)

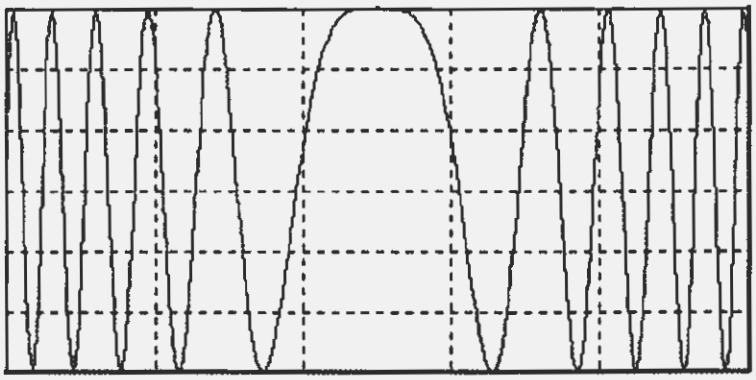

(a)

(a.u.)

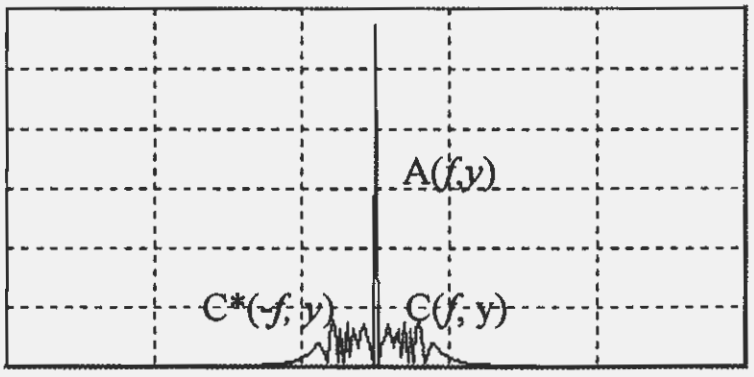

(b)

(a.u.)

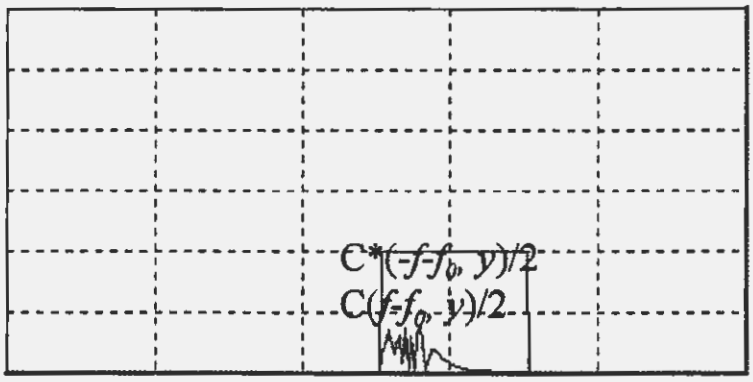

(c)

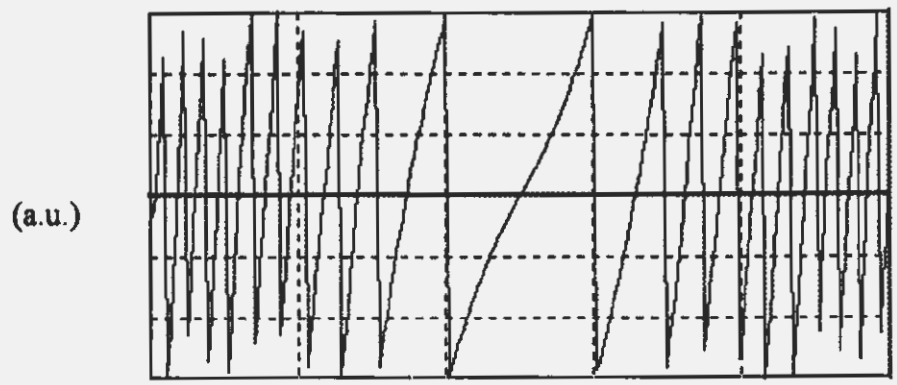

Figure 1.2

(a.u.)

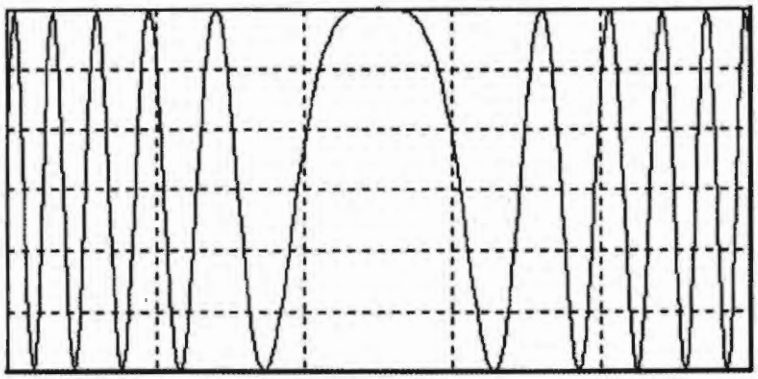

(a)

(a.u.)

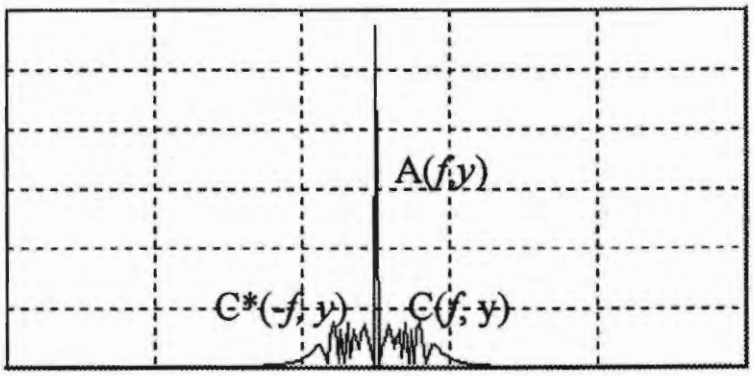

(b)

(a.u.)

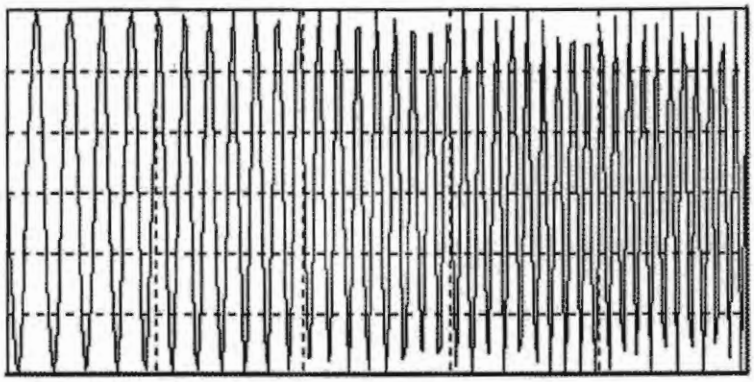

(c)

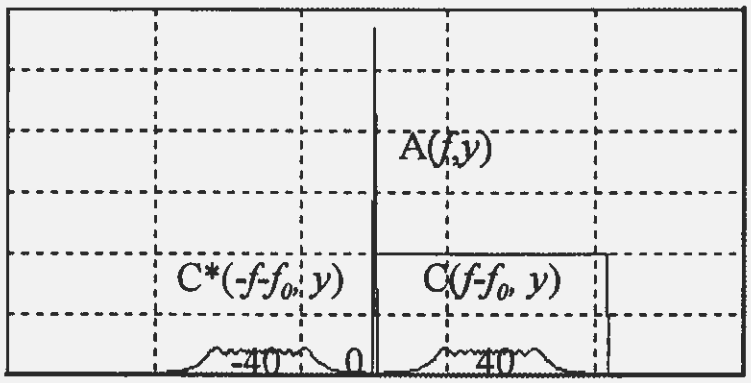

(d)

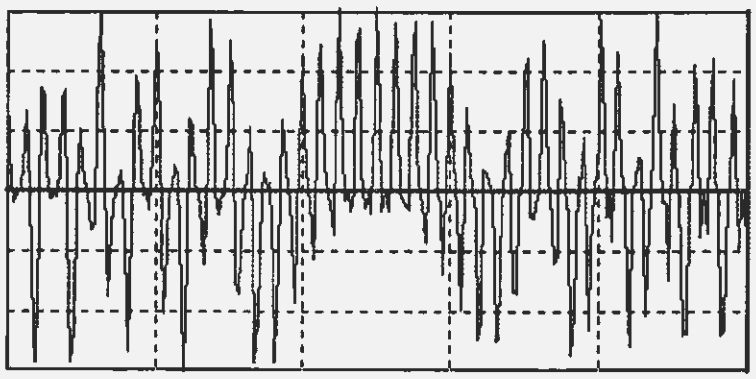

(e)

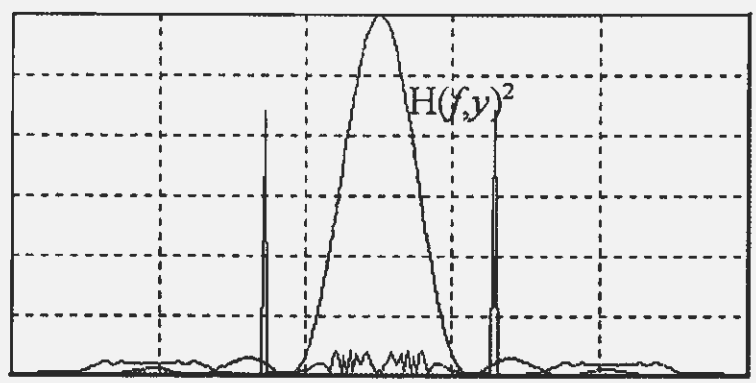

(f)

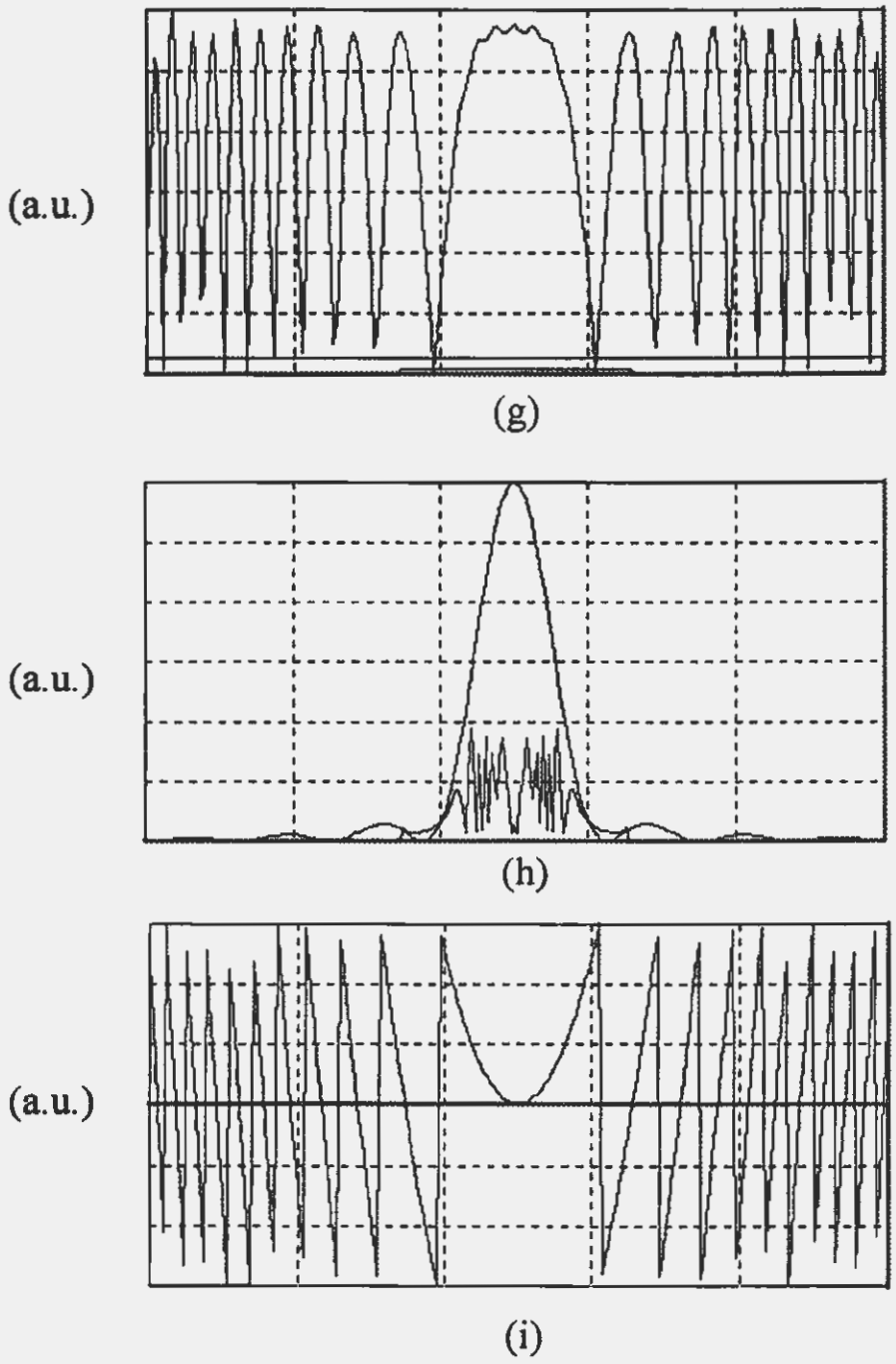

Figure 1.3

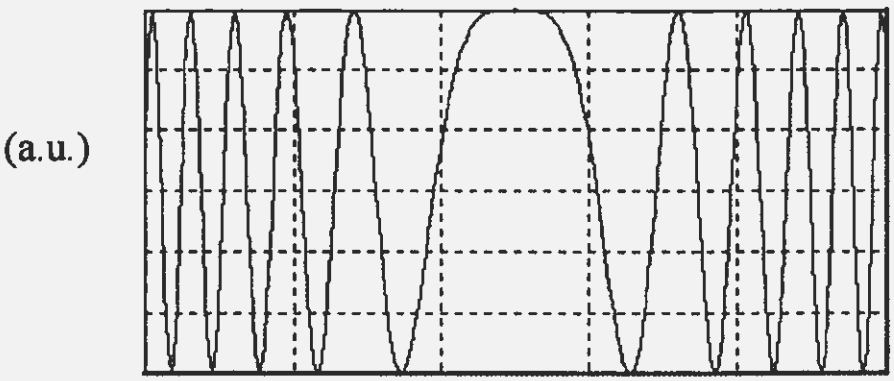

(a)

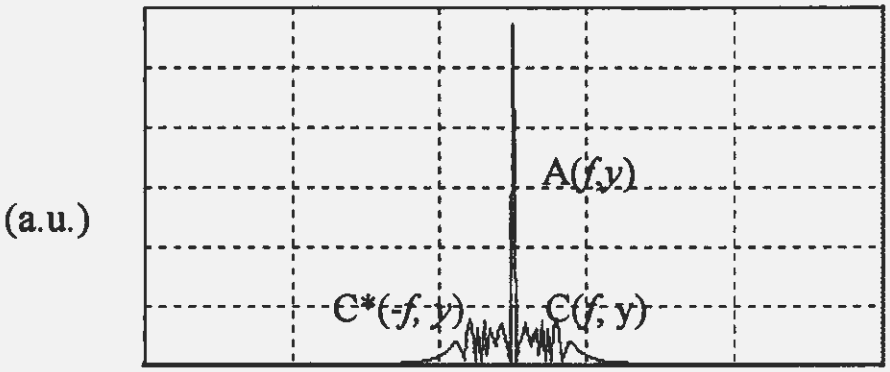

(b)

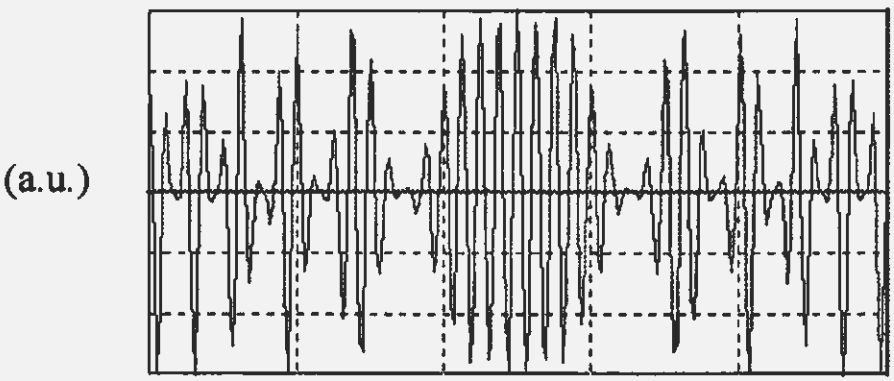

(c)

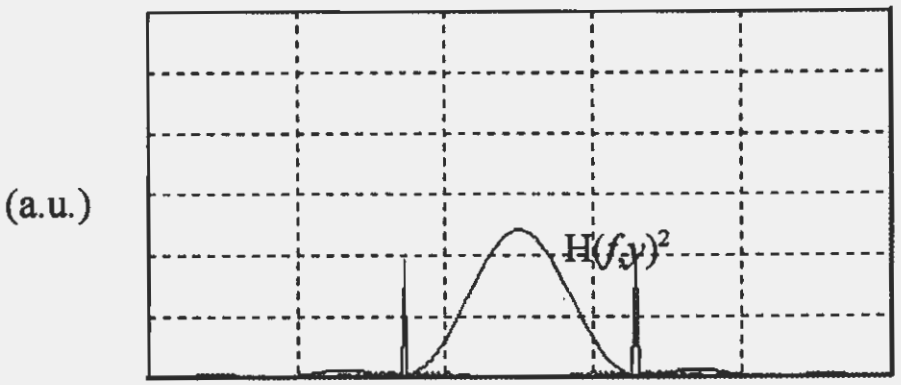

(d)

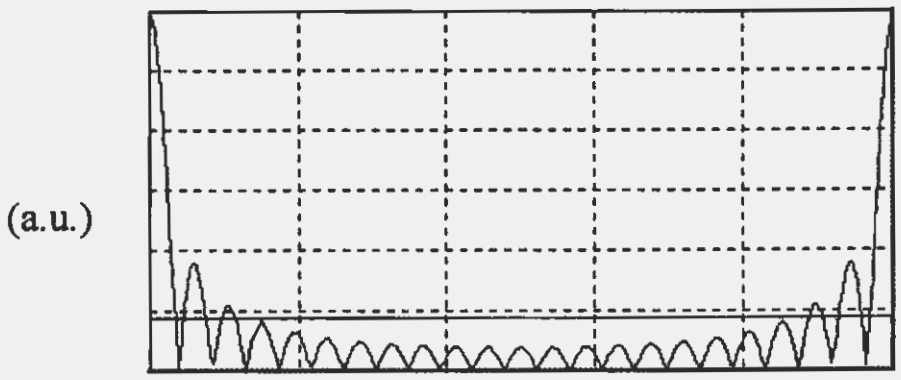

(e)

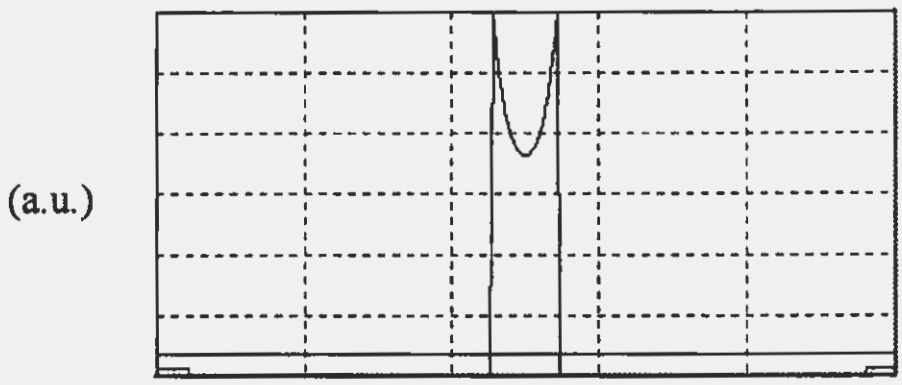

(f)

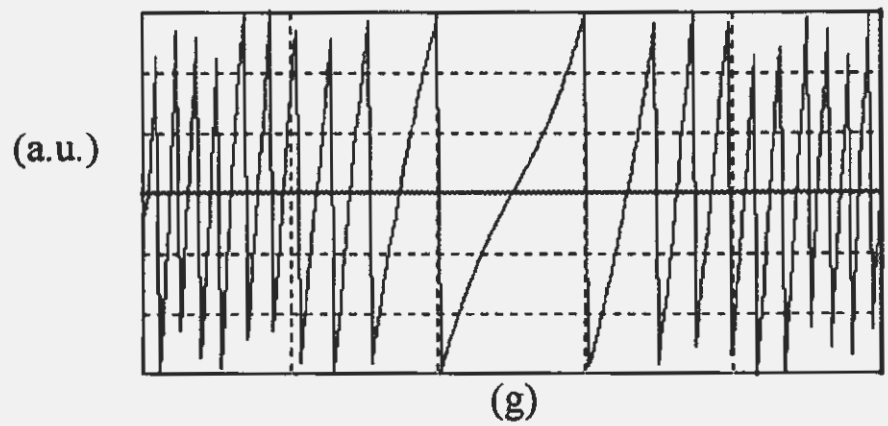

Figure 1.4

Chapter II

Analysis of Interferograms with a Spatial Radial Carrier

2.1 INTRODUCTION

The introduction of a linear carrier in an interferogram in order to avoid closed loop fringes is well known. The phase determination, called here demodulation, of these carrier frequency interferograms has been performed by Womak [1] in the spatial domain. The interferogram demodulation to obtain the phase or wavefront shape was done multiplying the interferogram by two perfect interferograms with the same linear carrier but with the two systems of fringes orthogonal to each other, in the sense that the phase difference between these two interferograms is 90°. The second step is to low pass filter the results of these two multiplications. Finally, the tangent of the phase is the ratio of these two filtered images.

Also, Takeda *et al* [2] proposed a Fourier Method to demodulate the interferogram with linear carrier, by performing a Fourier Transform of the interferogram. Then the first order lobe in the Fourier phase is isolated from the rest. To complete the process the inverse Fourier transform is taken, obtaining the desired wavefront slope.

We may have an interferogram of closed fringes in which to introduce the linear carrier is not practical for any reason, for example, because the minimum needed carrier is of such a high spatial frequency that the Nyquist limit is exceeded in the recording device. This situation can arise when the wavefront under measurement is highly aspheric or aberrated. In this case the demodulation has to be performed without the linear carrier. It is not always possible or convenient to introduce a linear carrier to form a system of open fringes. In this case the interferogram has to be demodulated with the presence of closed fringes. A Fourier method to demodulate in the interferogram has been proposed by Kreiss [3,4]. Later, a method to demodulate in the interferogram plane that do not require any kind of carrier, was proposed by Moore and Mendoza-Santoyo [5]. Moreover Servín *et al* [6] introduced another way of demodulating closed fringes interference patterns by the use of a regularized phase tracking technique. The main disadvantages of this procedure is its sequential nature which may propagate a detection error found in a place of the interferogram throughout the whole fringe pattern.

Peng *et al*[7] who were concerned by circular carrier, used a spatial phase shifting technique to demodulate the interferogram. However, to avoid closed fringes they also introduced an additional linear carrier.

The general problem of demodulating an interferogram with linear and circular carrier has been mathematically treated by Vlad and Malacara[8], and by Malacara *et al*[9].

Two methods to demodulate an interferogram with open or closed fringes, from a point of view of holography are described. This model gives us a good insight of these procedures and of their strong similarities. Some examples are presented.

2.2 INTERFEROGRAMS WITH A RADIAL OR CIRCULAR CARRIER

Closed system of fringes appear quite frequently when measuring mechanical components. The deformations in these cases may be as large that the introduction of a linear carrier to open the fringes would produce extremely high spatial frequencies. In this case the fringes have to be demodulated containing closed fringes.

A slightly different case arises when testing an spherical surface with nearly rotational symmetry. In this case a circular carrier, as pointed out by Vlad and Malacara [8] can be a proper solution. Then, a nearly centered system of rings appear.

The mathematical produce to demodulate these fringe patterns can be carried out in several manners. However, a holographic model illustrate several interesting properties and possible sources of errors. The holographic analogy also provides useful insight into the nature of the demodulation process.

A circular carrier, is introduced with a large defocusing, as shown in the computer simulated interferogram in Fig. 2.1 (a). Then, the irradiance function or signal $s(x,y)$ in the interferogram produced by the interference between a reference spherical wavefront and the wavefront under test is:

$$
\begin{aligned}
s(x, y) &= a + b \cos k\,[D(x^2 + y^2) - \phi(x, y)] \\
&= a + b \cos k[DS^2 - \phi(x, y)] \\
&= a + \frac{b}{2} e^{+ik[DS^2 - \phi(x, y)]} \\
&\quad + \frac{b}{2} e^{-ik[DS^2 - \phi(x, y)]}
\end{aligned}
\tag{2.1}
$$

where a is the background illumination, b is the fringe contrast, k is the magnitude of the wave vector, D is the defocusing coefficient, ϕ is the wavefront under test, and $S^2 = x^2 + y^2$.

The radial carrier spatial frequency $f(x,y)$ is

$$
f(x, y) = \frac{2\,D\,S}{\lambda} \tag{2.2}
$$

For academic purposes a holographic analogy is used to interpret the interferogram as an on-axis or Gabor hologram. This hologram can be demodulated by illuminating it with *a*) a spherical reference wavefront or *b*) with a flat reference wavefront. This demodulation may be achieved only if the phase in the irradiance function increases or decreases in a monotonic manner from the center toward the edge of the pupil. Thus, if the defocusing term is positive, we require that

$$
\frac{\partial\,[DS^2 - \phi(x, y)]}{\partial\,S} > 0 \tag{2.3}
$$

or

$$D > \frac{1}{2S} \frac{\partial \phi(x, y)}{\partial S} \tag{2.4}$$

For all values of S inside the pupil. To say this in words, the carrier fringes should have a bandwidth adequate to contain the wavefront distortion.

This condition assures us that there are not two fringes in the interferogram aperture with the same order of interference. In other words, no fringe crosses more than once any line traced from the center of the interferogram to its edge.

In the vicinity of the center of the interferogram the circular carrier frequency is so small that the demodulated phase in this region is not fully reliable. This is a small disadvantage of this method. To reduce this problem, the circular carrier frequency should be as large as possible, provided the Nyquist limit is not exceeded.

2.3 PHASE DEMODULATION OF CLOSED FRINGE PATTERNS

The phase demodulation of the interferogram (hologram reconstruction) with a circular carrier can be performed using an on-axis spherical reference wavefront as well as with a tilted flat reference wavefront. Next, these two methods, although quite similar, have some important differences, as will be described.

2.3.1 Phase Demodulation with a Radial Reference Carrier (Spherical Reference Wavefront)

In this case we assume that the interferogram is formed by a perfect spherical wavefront and a nearly flat, aberrated wavefront. The demodulation can be performed using an on-axis spherical reference wavefront with almost the same curvature used to introduce the circular carrier as illustrated in Fig. 2.2.

Then the amplitude $r(x,y)$ of the non aberrated spherical reference wavefront may be

written as

$$\begin{aligned} r(x, y) &= e^{i[k D_r (x^2 + y^2)]} \\ &= e^{i[k D_r S^2]} \end{aligned} \tag{2.5}$$

Where the curvature of this wavefront is close to that of the original spherical wavefront that produced the hologram (circular carrier). In other words, the value of the defocusing coefficient D_r for the reference beam must be as close as possible to the value of the defocusing coefficient D for the spherical beam introducing the circular carrier.

The product between the interferogram irradiance $s(x, y)$ and the illuminating wavefront $r(x, y)$ is

$$\begin{aligned} r(x, y)\, s(x, y) &= a\, e^{i[k D_r S^2]} \\ &+ \frac{b}{2} e^{ik[(D + D_r)S^2 - \phi(x, y)]} \\ &+ \frac{b}{2} e^{-ik[(D - D_r)S^2 - \phi(x, y)]} \end{aligned} \tag{2.6}$$

The first term is the zero order beam corresponding to the illuminating spherical wavefront. Its spatial frequency $f_r(x,y)$ is zero at the center of the fringes and increases with the square of S toward the edge of the pupil, as.

$$f_r(x,y) = \frac{2 D_r S}{\lambda} \tag{2.7}$$

The width of this zero order lobe in the Fourier space is $2D_rS_{max}/\lambda$. The second term is the minus first order. It is the conjugate wavefront with opposite deformations to those of the

wavefront under test. Its curvature is about twice the reference wavefront curvature and its spatial frequency $f_{-1}(x,y)$ is

$$f_{-1}(x,y) = \frac{2\,(D + D_r)\,S}{\lambda} - \frac{1}{\lambda}\,\frac{\partial\phi(x,\,y)}{\partial\,S} \tag{2.8}$$

The bandwidth of this minus one order lobe is $2(D+D_r)S_{max}/\lambda$ if the wavefront aberrations are small compared with the defocus. The third term is the first order of diffraction and represents the reconstructed wavefront, with only a slight difference in curvature and its spatial frequency $f_{+1}(x,y)$ is

$$f_{+1}(x,y) = \frac{2\,(D - D_r)\,S}{\lambda} - \frac{1}{\lambda}\,\frac{\partial\phi(x,\,y)}{\partial\,S} \tag{2.9}$$

The width of this plus one order lobe is very small if $D \sim D_r$ and the wavefront deformations are small. The Fourier spectra of these three beams are concentric and overlap each other. However, the wavefront to be measured (order plus one) can be isolated with small contributions from the other two lobes remaining, due to the different diameters of their spectra. Equation 6 can also be written

$$\begin{aligned} s(x,y)\;r(x,y) &= z_C(x,y) + i\,z_S(x,y) \\ &= s(x,y)\;\cos\,[kD_rS^2] + i\,s(x,y)\;\sin\,[kD_rS^2] \end{aligned} \tag{2.10}$$

We see that the phase demodulation of an interferogram with a circular carrier can be performed by multiplying the signal by these reference cosine and sine functions with a quadratic phase (defocus), close to that used to introduce the circular carrier ($D \sim D_r$).

Using a two dimensional digital low-pass filtering with narrow band, the contribution from the first two terms in Eq. 6 are almost eliminated, obtaining:

$$\bar{z}_C(x, y) + i\,\bar{z}_S(x, y) = \frac{b}{2}\, e^{-ik[(D - D_r)S^2 - \phi(x, y)]}$$

$$= \frac{b}{2}\cos k[(D - D_r)S^2 - \phi(x, y)]$$

$$- i\frac{b}{2}\sin k[(D - D_r)S^2 - \phi(x, y)] \qquad (2.11)$$

Thus, the wavefront under reconstruction is given by

$$k[(D - D_r)S^2 - \phi(x, y)] = -\tan^{-1}\frac{\bar{z}_S(x, y)}{\bar{z}_C(x,y)} \qquad (2.12)$$

As an example, a computer simulated interferogram with a circular carrier and its Fourier transform is in Fig. 2.1 (a) and (b) which has a resolution of 128 by 128 pixels with 256 gray levels. The circular carrier of reconstruction and the demodulated phase map are in Fig. 2.3 (a) and (b) respectively. Its corresponding unwrapped wavefront is shown in Fig. 2.3 (c). The circular carrier is large enough so that the plus one order isolation can be achieved with 40 passes with a 3x3 square low pass convolution filter. If the circular carrier is low, the filter has to be relatively narrow band-width to isolate the central lobe in the Fourier spectrum as much as possible.

The filtering process presented in this section eliminates only those zones in the undesired wavefronts (orders 0 and -1) that have a slope (spatial frequency in the Fourier plane) greater than the maximum slope in the wavefront under measurement (order +1). Thus, a small region with low spatial frequency near the center of the nearly circular fringes is less properly demodulated. This is not a serious problem, however in astronomical optics, where the central region is frequently not used. The
diameter of this circular undermodulated zone is reduced (but in principle never completely

eliminated) if a higher frequency for the circular carrier is used. When a large number of convolutions iterations are performed (*e.g.* 400), with the same filter as in Fig. 2.3, the filtering process approaches its ideal limit and the central error is practically removed. However, we must be careful not to over filter, because some spatial frequencies really present in the wavefront may also be removed. Another possible source of errors around the edge is due to imperfect filtering where the edge pixels do not have eight neighboring pixels, but this occurs only very close to the edge.

This numerical simulation is presented in Fig. 2.4.

2.3.2 Phase Demodulation with a Linear Reference Carrier (Tilted Plane Reference Wavefront)

In this case we assume that the interferogram is formed by a perfectly flat wavefront and a defocused aberrated wavefront. With a different point of view, the principle of this method was described by Moore and Mendoza-Santoyo[2] which is basically a modification of that of Kreis[3,4] using the Fourier method. We will consider here a circular carrier, but we will see that the method is more general and also applies to interferograms containing closed fringes.

To understand how the demodulation can be made with closed fringes, using the holographic model, let us consider the interference along one diameter in an interferogram with a circular carrier. In Fig. 2.5(a) we have a flat wavefront interfering with a spherical wavefront. In Fig. 2.5(b) the spherical wavefront has been replaced by a discontinuous wavefront in which the sign of the left half has been reversed. Both pairs of wavefronts produce the same interferogram, with the same signal as in Fig. 5(c).

In the first case the phase increases monotonically from the center to the edge. In the second case the phase increases monotonically from the left to the right. If we assume that what we have is the second case, we can phase demodulate in the standard manner, multipliying by the reference sine and cosine functions and then low pass filtering these two functions. However, to obtain the correct result we must reverse the sign of the left half of

the demodulated wavefront.

Using again the holographic analogy, let us consider an interferogram with a circular carrier, illuminated with a tilted plane wavefront as illustrated in Fig. 2.6. This illuminated tilted plane reference wavefront may be written as

$$\begin{aligned} r(x,y) &= e^{i(2\pi f_r x)} \\ &= \cos(2\pi f_r x) + i \sin(2\pi f_r x) \end{aligned} \tag{2.13}$$

Where this reference (reconstructing) tilt has to be larger than half the maximum tilt in the wavefront, along the x axis. Figure 2.6(a) shows the reconstruction with the minimum reference frequency (tilt of reconstructing wavefront) and with a larger frequency in Fig. 2.6(b).

The product between the interferogram irradiance $s(x,y)$ in Eq. 1 and the illuminating wavefront amplitude $r(x,y)$ is

$$\begin{aligned} s(x,y)\, r(x,y) = {} & a\, e^{i[2\pi f_r x]} \\ & + \frac{b}{2} e^{i[2\pi f_r x + k(DS^2 - \phi(x,y))]} \\ & + \frac{b}{2} e^{-i[-2\pi f_r x + k(DS^2 - \phi(x,y))]} \end{aligned} \tag{2.14}$$

The first term is the tilted flat wavefront (zero order). The second term is the conjugate wavefront and, the last term is the reconstructed wavefront to be measured. The wavefront to be measured and the conjugated wavefront differs only in the sign of the deformations with respect to the reference plane.

The Fourier spectrum of expression 14 is illustrated in Fig. 2.7. We see that these

three spots are concentric, but shifted laterally with respect to the axis.

If we use a rectangular low pass filter as shown in the right side of Fig. 2.7, we can see that we are isolating the reconstructed wavefront for the positive y half-plane and the conjugate wavefront for the negative y half-plane. The width of the filter in the y direction should be quite long. Thus, if a convolution mask is used to low pass filter, a Nx1 elements mask is appropriate. The square convolution filter was convolved with the image so many times that the resulting filter has a gaussian shape. Because of this, the resulting estimated phase has minimum ringing.

The conjugate wavefront is equal in magnitude to the reconstructed wavefront, only with the opposite sign. Thus, we obtain the wavefront under measurement by just changing the sign of the retrieved wavefront deformations for the negative half plane. It is easy to understand that there are singularities in the vicinity of the points where the slope of the fringes is zero.

We can also write expression 14 as

$$\begin{aligned} s(x,y)\ r(x,y) &= z_C(x,y) + i\, z_S(x,y) \\ &= s(x,y)\ \cos(2\pi f_r x) + i\, s(x,y)\ \sin(2\pi f_r x) \end{aligned} \tag{2.15}$$

Again, we see that the phase demodulation of an interferogram with a circular carrier can be done by multipliying the signal by the cosine and sine functions with a reference frequency. This reference frequency has to be larger than half the maximum spatial frequency in the interferogram and the filter edge in the Fourier domain has to be sharp enough to reject the zero order as much as possible.

$$\bar{z}_C(x,y) + i\,\bar{z}_S(x,y) = \frac{b}{2}\, e^{-i[-2\pi f_x x + k(DS^2 - \phi(x,y))]} =$$

$$\frac{b}{2}\cos\,[-2\pi f_x x + k(DS^2 - \phi(x,y))] -$$

$$i\,\frac{b}{2}\sin\,[-2\pi f_x x + k(DS^2 - \phi(x,y))] \qquad (2.16)$$

Using a one dimensional digital low-pass filtering along the direction where the carrier is introduced the first two terms in Eq. 14 are eliminated, obtaining:

Thus, the retrieved phase is given by:

$$[-2\pi f_x x + k(DS^2 - \phi(x,\, y))] = -\tan^{-1}\frac{\bar{z}_S(x,\, y)}{\bar{z}_C(x,y)} \qquad (2.17)$$

which, as we know, give us the wavefront to be measured by changing the sign of the phase for negative values of y.

The example of interferogram with a circular carrier and its Fourier transform is again in Fig. 2.1.

Fig. 2.8(a) shows the linear carrier used to demodulate the interferogram shown in Fig. 2.1(a). To perform the low pass filtering depicted in Fig. 2.7 we have convoluted 30 times a 3x1 averaging filter. The detected phase map shown in Fig. 2.8(b) was obtained as the phase of this low pass filtered complex image. As we can see from Fig. 2.8(b) the sign of one side of the phase map is reversed. This constitutes the main drawback of this method. Nevertheless one may still use this method if the wrong phase sign is reversed.

2.4 THE METHOD PROPOSED BY GARCIA-MARQUEZ *et al.* A REVIEW

García-Márquez *et al* were concerned on a space domain method with a radial (square) carrier frequency instead the linear one. From eqn. (2.1) to eqn. (2.12) the method is mathematically explained. Now, the graphical method is exposed.

As the circular carrier is large enough so that the plus one order isolation can be achieved with n passes with a 3x3 square low-pass convolution filter. As result of this concurrent application, the filter has a gaussian shape, avoiding the introduction of spurious high frequencies. In Fig. 2.9 it is shown how a $\mathrm{sinc}^n x$ function narrows from a ringing behaviour to a sharp shape.

2.5 ANALYSIS OF ERROR AND ITS SOURCES

Next, an analysis of the root means square (RMS) and maximum error is presented.

2.5.1 RMS and Maximum Error with a Square Filters

In order to compute the RMS wrapped error the following equation[11] is used

$$RMS_w = \left(\frac{\sum_{i=1}^{N} \left[[(D - D_r)S^2 - \phi(x, y)] - \phi(x,y) \right]^2_w}{N-1} \right)^{1/2} \qquad (2.18)$$

where RMS_w represents the RMS wrapped error in the retrieved phase. Figure 2.11 shows this error when a 3x3 low-pass convolution filter is used with two different number of passes Where RMS_w represents the RMS wrapped error in the retrieved phase. Figure 2.11 shows

this error when a 3x3 low-pass convolution filter is used with two different number of passes. This graphic of RMS error is only presented for illustrative purposes. Figure 2.12 shows a graphic representing both error analysis and table 1 indicates the number of passes needed to get the lower either RMS or maximum error.

Table 1.-Evolution of some errors as a function of the number of passes with a 3x3 low-pass filter.

Number of passes	**RMS with a, 3x3 filter**	**max. error, 3x3 filter**
1	1.2537	3.1408
40	0.2441	2.9968
80	0.1827	1.0639
85	**0.1824**	1.0263
95	0.1835	**0.9665**
100	0.1848	0.9702
400	0.3515	1.7267

2.5.2 Recursive Method for Radial Reference Carrier Demodulation

It is also possible to reduce the error by using a recursive method when demodulating the phase with a radial reference carrier. For the readers' convenience eqn. (2.10) may be written as follow

$$Z_c = b\cos(DS^2+\phi)\cos(D_rS^2)\,,$$
$$Z_s = b\cos(DS^2+\phi)\sin(D_rS^2) \qquad (2.19)$$

and

$$\hat{\phi} = \tan^{-1}\left[\frac{h * z_S(x, y)}{h * z_C(x,y)}\right]. \tag{2.20}$$

We will use the first estimation of the wavefront as a new reference according to

$$\begin{aligned} Z_{c_1} &= b\cos(DS^2+\phi)\cos(D_rS^2+\hat{\phi}), \\ Z_{s_1} &= b\cos(DS^2+\phi)\sin(D_rS^2+\hat{\phi}) \end{aligned} \tag{2.21}$$

and the wrapped error between the first and the second iteration is given by

$$\phi_e = \tan^{-1}\left[\frac{h * z_{S_1}(x, y)}{h * z_{C_1}(x,y)}\right]. \tag{2.22}$$

The newly estimated phase is then given by summing the error phase to the first estimation,

$$\hat{\phi}_e = \phi - \hat{\phi}_1, \tag{2.23}$$

the same procedure may be used several times until the phase error becomes neglectible.

$$\phi = \hat{\phi}_1 + \hat{\phi}_e \tag{2.24}$$

When using a circular carrier demodulation, we have some problems in the detection of the true phase due to the erroneous phase information in the center of the interferogram. But, when a large number of convolution iterations are made, this error is practically removed. This problem may be attenuated with a large number passes with the rectangular

convolution filter.

On the other hand, if we want that this problem to be avoided, we can demodulate by introducing a reference linear carrier. Then, by doing the appropriate change on the sign in the recovered phase, this error in the center of the interferogram could be removed. In addition to this, we have also talk about the importance of using an appropriate Nx1 convolution mask to low pass filter, in order to obtain a good demodulation

2.6 REFERENCES

[1] K. H. Womack, "Interferometric phase measurement using spatial synchronous detection," in *Opt. Eng.*, **23**, 391-395 (1984).

[2] M. Takeda, H. Ina and S Kobayashi, "Fourier-transform method of fringe-pattern analysis for computer-based topography and interferometry," *J. Opt. Soc. Am*, **72** 156-160 (1982).

[3] T. Kreis., "Digital holographic interference-phase measurement using the Fourier transform method," *J. Opt. Soc. Am. A.*, **3**, 847-855 (1986).

[4] T. Kreis., "Fourier transform evaluation of holographic interference patterns," *Proc. SPIE.*, **814**, 365-371 (1987).

[5] A. J. Moore and F. Mendoza-Santoyo, "Phase demodulation in the space domain without a fringe carrier," *Opt. and Lasers in Eng.*, **23**, 319-330 (1995).

[6] M. Servín, J. L. Marroquín, and F. J. Cuevas, "Demodulation of a single interferogram by use of a two-dimensional regularized phase-tracking technique," *Appl. Opt.*, **36**, 4540-4548 (1997).

[7] X. Peng, S.M. Zhou and Z. Gao, "An automatic demodulation technique for a non-linear carrier fringe pattern," *Optik*, **100**, 11-14 (1995).

[8] V. I. Vlad and D. Malacara, "Direct spatial reconstruction of optical phase from phase-modulated images," in *Progress in Optics*, Vol. XXXIII, Ed. E. Wolf (North-Holland, Amsterdam) 261-317 (1994).

[9] D. Malacara, M. Servín and Z. Malacara, "Interferogram Analysis for Optical Testing," Marcel Dekker, New York (1998).

[10] García-Márquez, J., D. Malacara-Hernández and M. Servín, "Analysis of interferograms with a spatial radial carrier or closed fringes, and its holographic analogy," *Appl. Opt.*, **37**, (1998).

[11] Taylor, J. R., "An Introduction to Error Analysis," University Science Books, Sausalito, CA, 97-101 (1982).

Figure Captions

Figure 2.1.- a) Computer simulated interferogram with a circular carrier in a 128x128 pixel's grid. b) spectrum.

Figure 2.2.- Phase demodulation in an interferogram with a circular carrier using a spherical reference wavefront.

Figure 2.3.- Results from demodulation of interferogram in Fig. 2.1. using a 3x3 averaging filter with 40 passes. a) Circular carrier or defocused reconstructing wavefront, b) phase map, c) unwrapped phase.

Figure 2.4.- Results from demodulation of the same interferogram as in Fig 2.3 but, using a 3x3 averaging filter with 400 passes. a) Circular carrier or defocused reconstructing wavefront,. b) phase map, c) unwrapped phase.

Figure 2.5.- Interfering wavefront, a) a flat wavefront and apherical wavefront, b) a flat wavefront. and a discontinuous wavefront with two spherical portions and c) signal for both cases.

Figure 2.6.- Phase demodulation in an interferogram with a circular carrier using a tilted plane reference wavefront. a) Minimum tilt, b) greater than minimum tilt.

Figure 2.7.- Fourier spectrum produced by an interferogram with a circular carrier (Gabor hologram) when illuminated with a tilted flat reference wavefront. The sign of the phase is

reversed for negative values of y.

Figure 2.8.- Demodulation of interferogram in Fig. 1 using a 3x1 convolution filter with 30 passes. a) Reference reconstructing frequency and b) phase map.

Figure 2.9.- Spatial Synchronous detection with fringe carrier, (a) intensity distribution $\phi(x,y)$, (b) its Fourier transform, (c) radial carrier DS^2 (d) interferogram $\phi(x,y) + DS^2$ (e) intensity distribution multiplied by carrier frequency, (f) its Fourier transform, (g) low-pass filter applied to (e), (h) unwrapped phase.

Figure 2.10.- Behaviour of a $\text{sinc}^n x$ function, (a) $n = 1$, (b) $n=3$, (c) $n=30$.

Figure 2.11.- RMS error (a) 40 passes, (b) 400 passes.

Figure 2.12.- RMS and maximum error versus the number of passes.

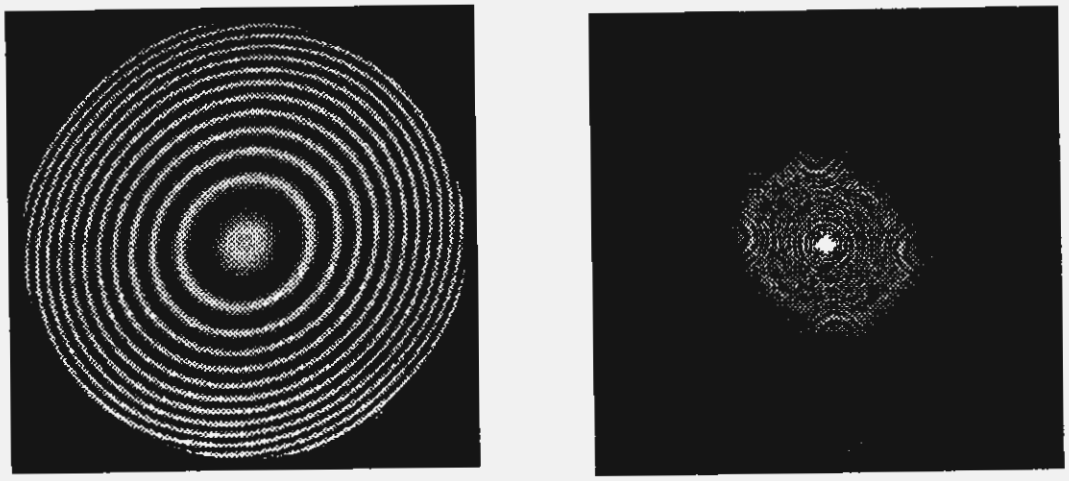

(a) (b)

Figure 2.1

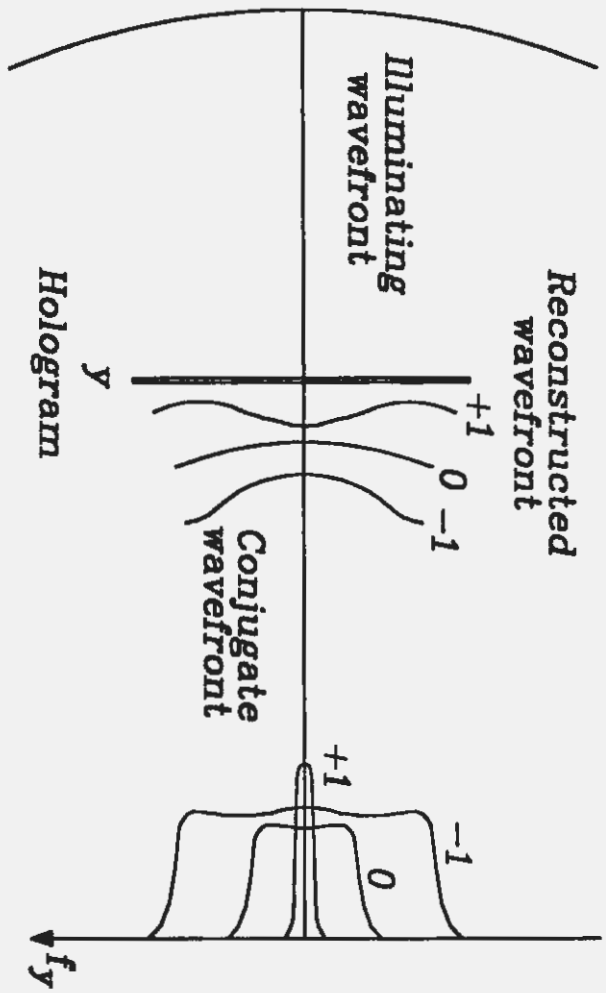
Reconstructed wavefront
Illuminating wavefront
y
Hologram
+1
0
−1
Conjugate wavefront
+1
−1
0
f_y

Figure 2.2

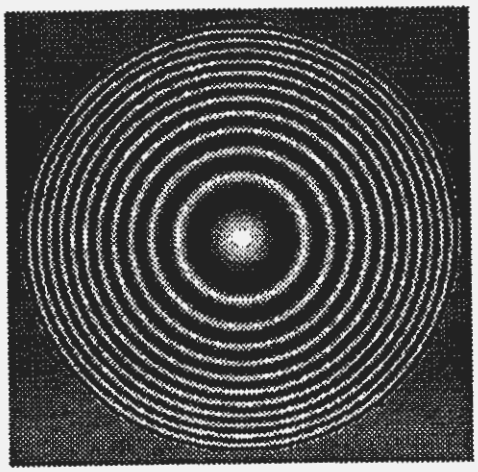

(a)

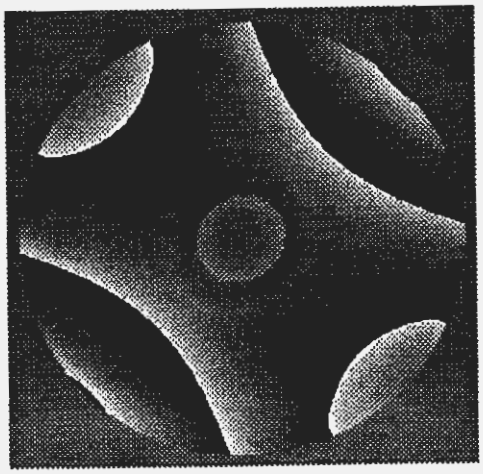

(b)

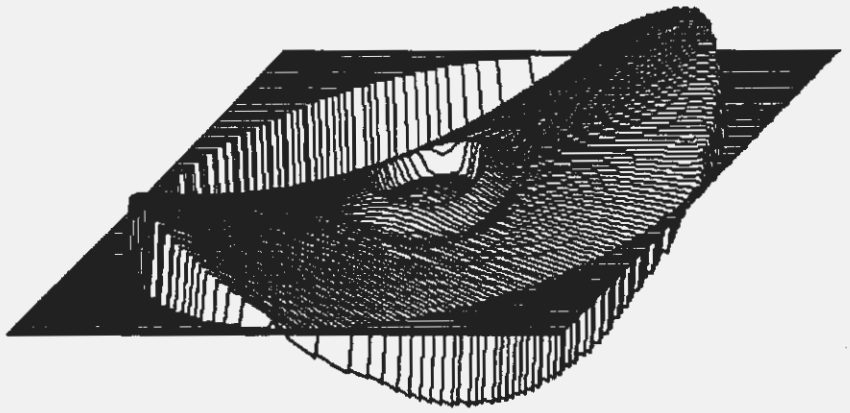

(c)

Figure 2.3

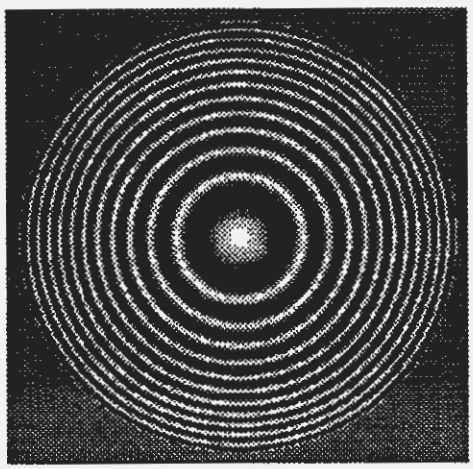

(a)

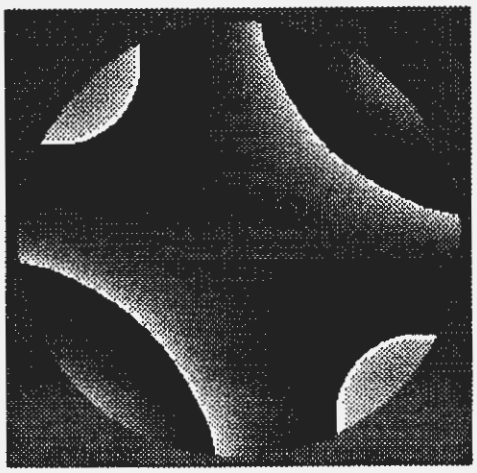

(b)

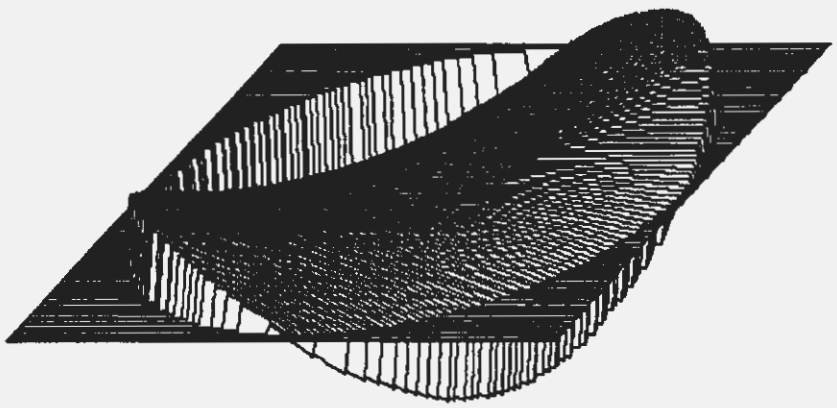

(c)

Figure 2.4

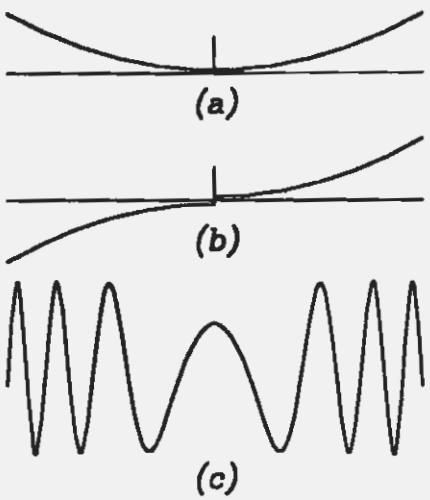

Figure 2.5

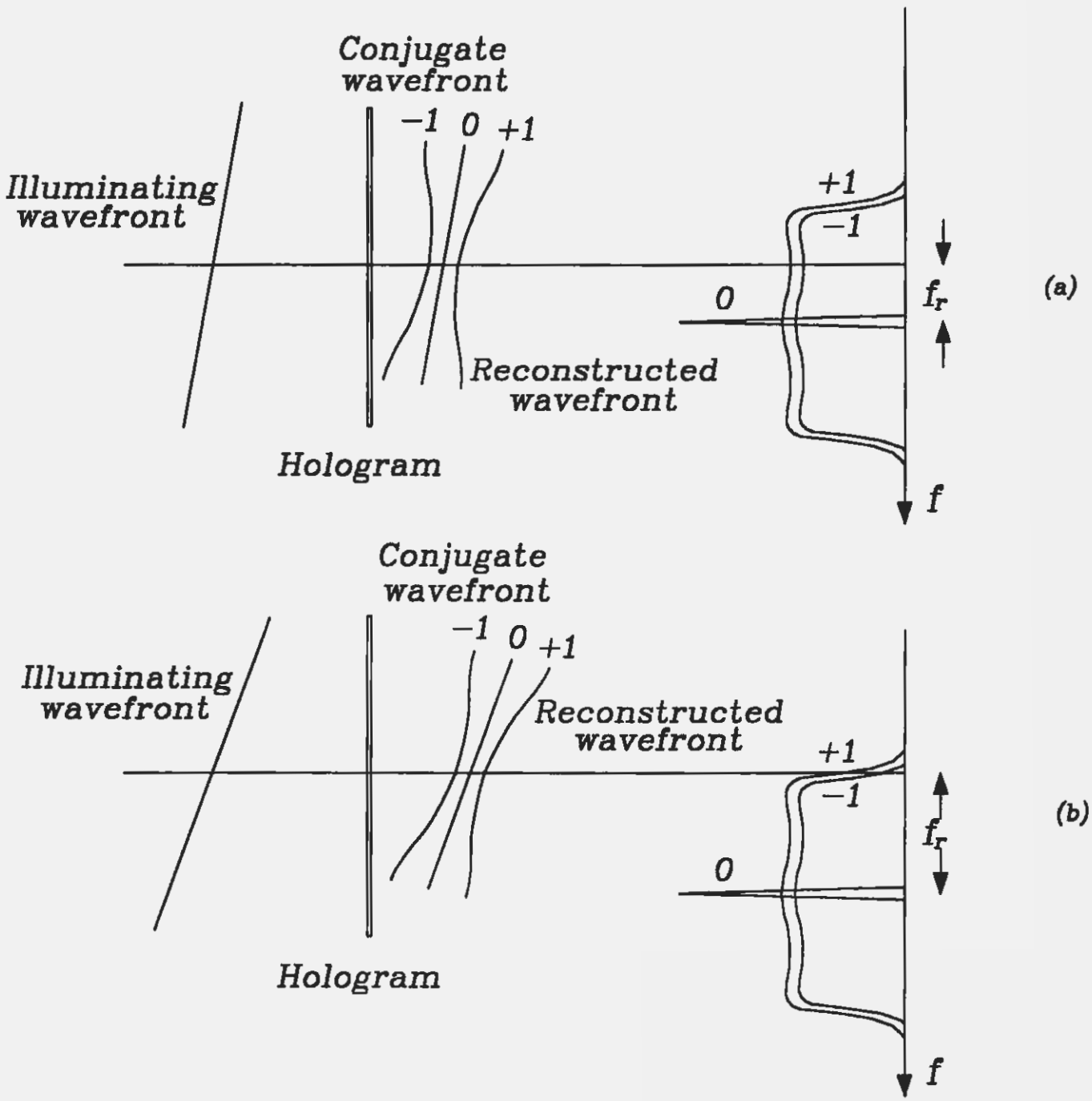
Conjugate wavefront
−1 0 +1
Illuminating wavefront
+1
−1
0
f_r
Reconstructed wavefront
Hologram
f
(a)
Conjugate wavefront
−1 0 +1
Illuminating wavefront
Reconstructed wavefront
+1
−1
0
f_r
Hologram
f
(b)

Figure 2.6

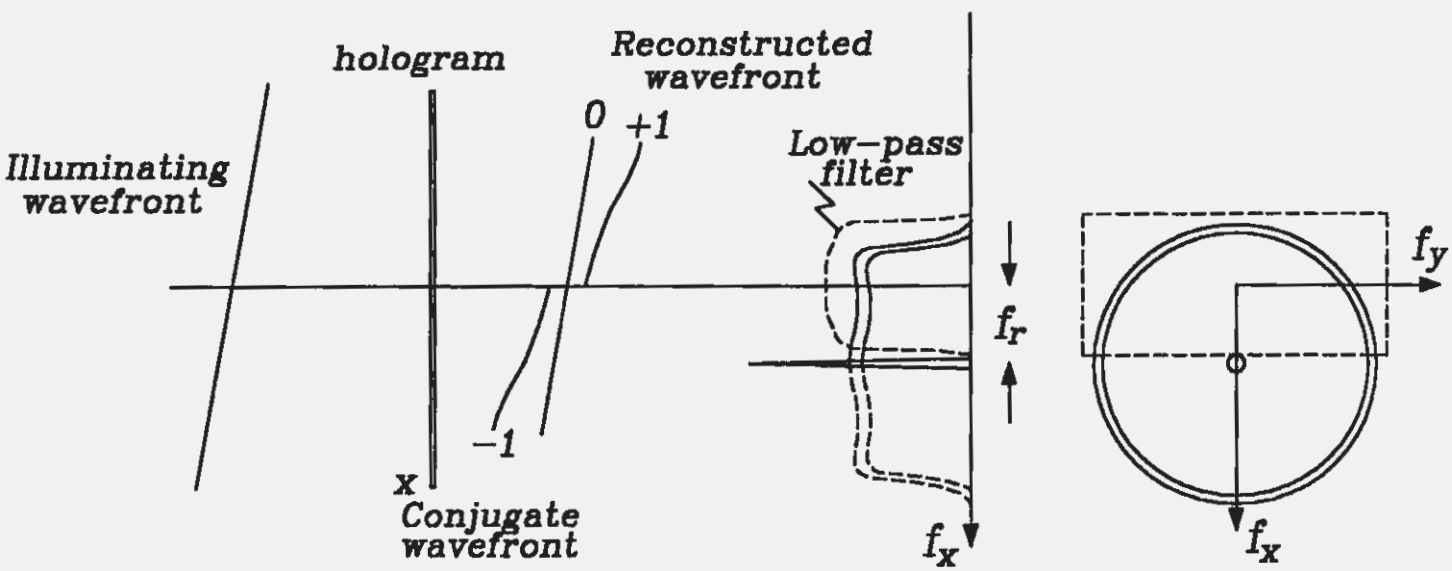
hologram
Reconstructed wavefront
0
+1
Illuminating wavefront
Low–pass filter
f_r
f_y
−1
x
Conjugate wavefront
f_x
f_x

Figure 2.7

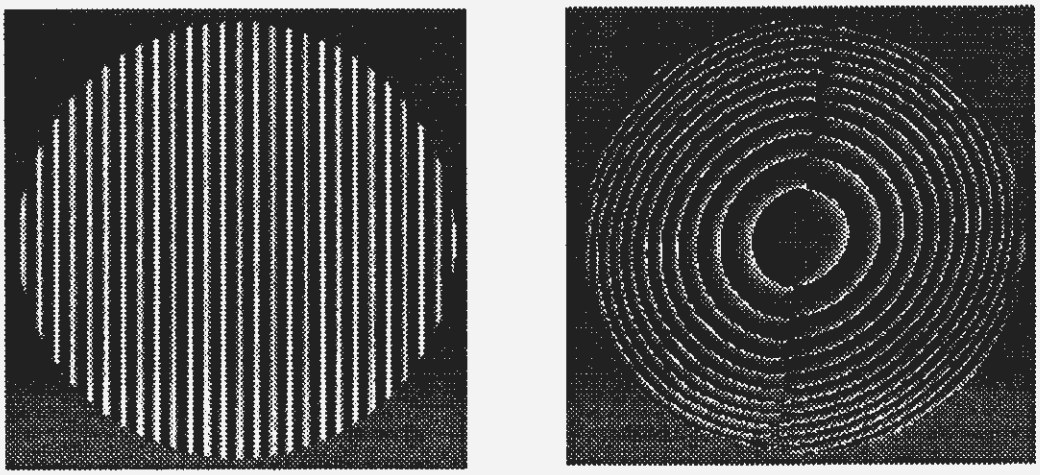

(a) (b)

Figure 2.8

(a.u.)

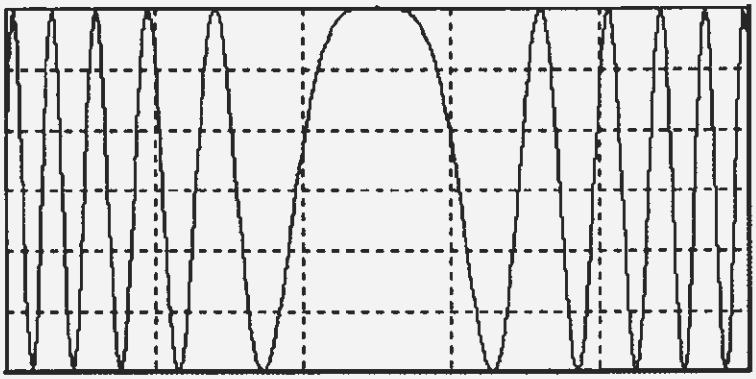

(a)

(a.u.)

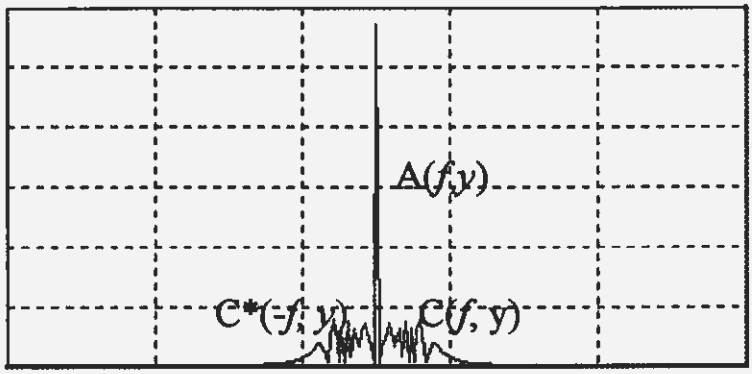

(b)

(a.u.)

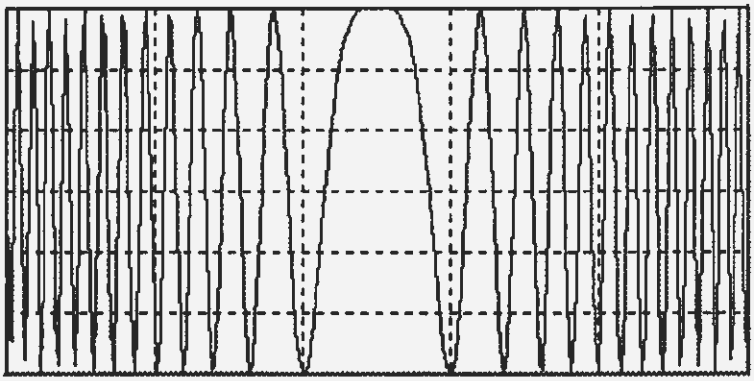

(c)

(a.u.)

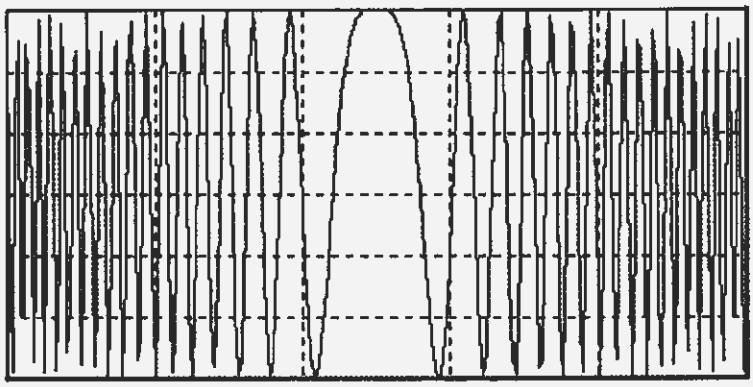

(d)

(a.u.)

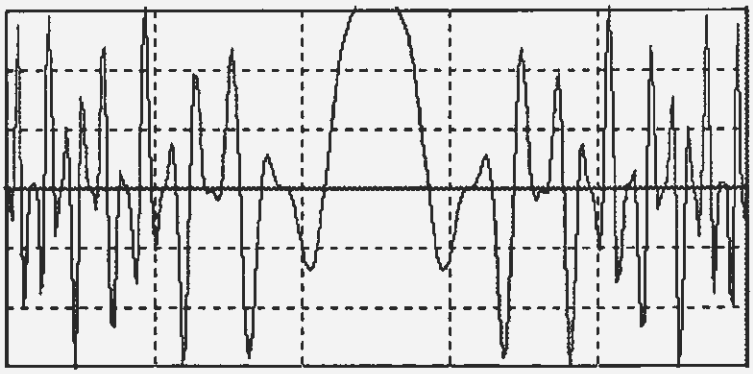

(e)

(a.u.)

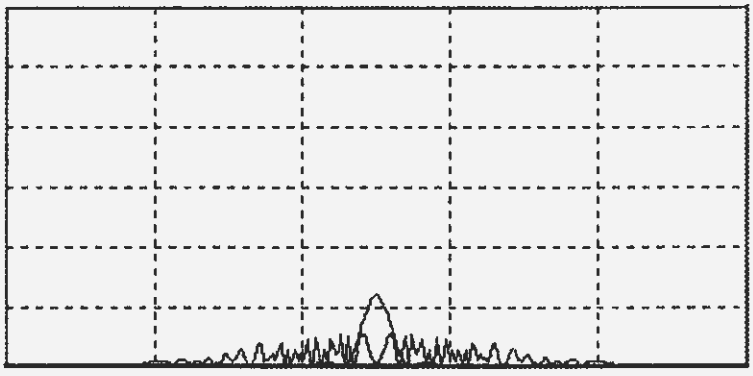

(f)

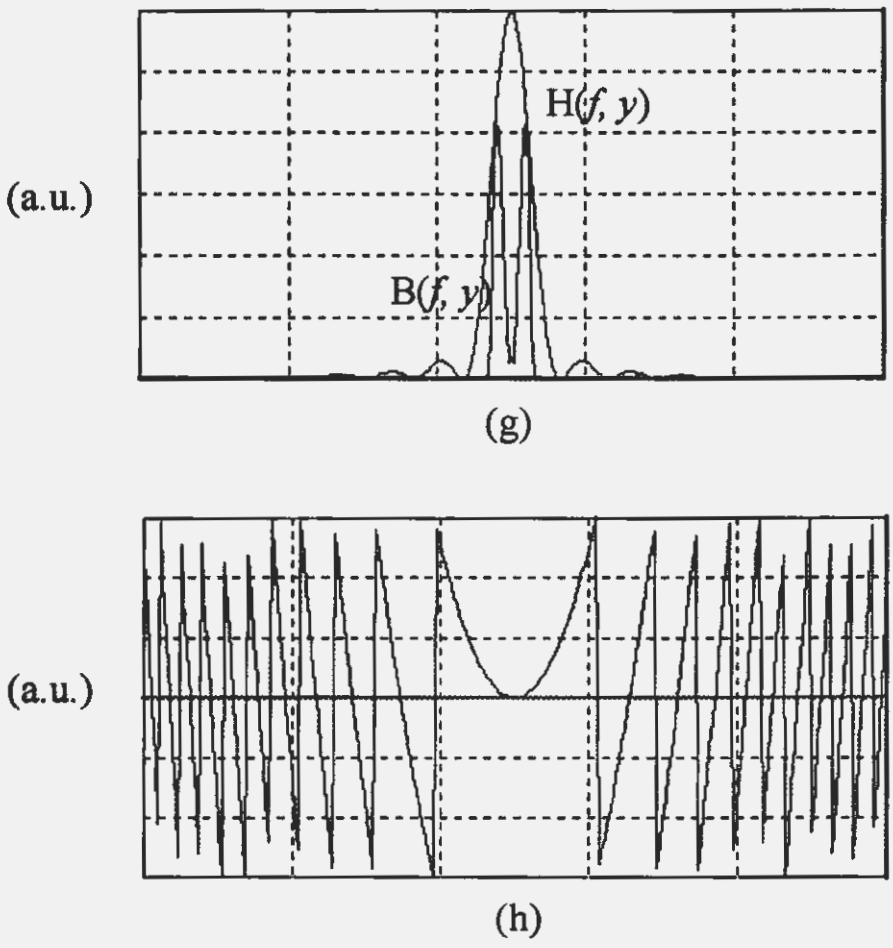

Figure 2.9.-

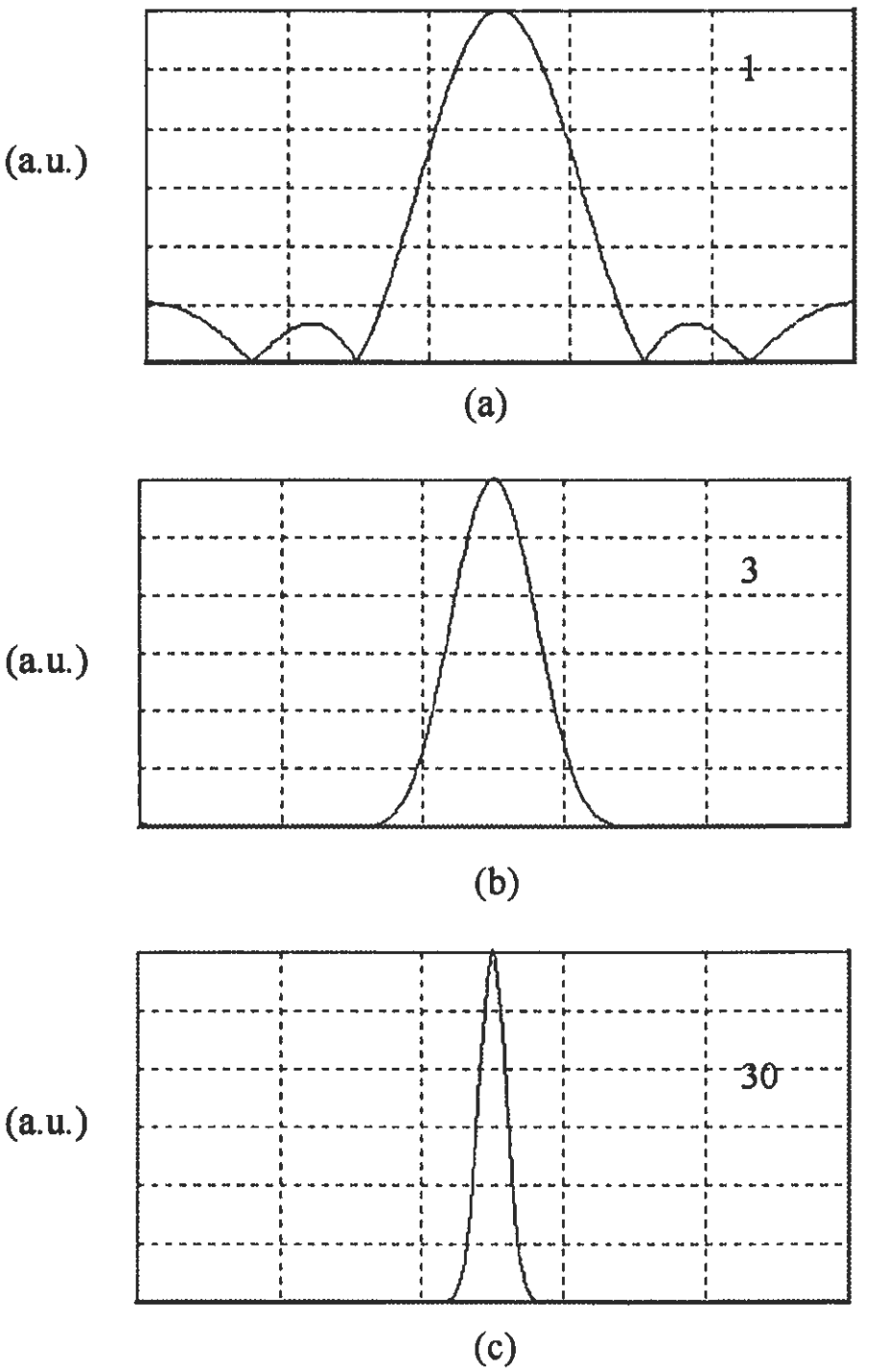

Figure 2.10.-

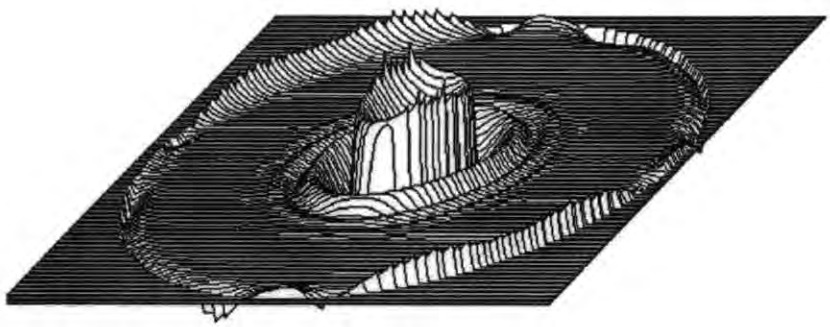

(a)

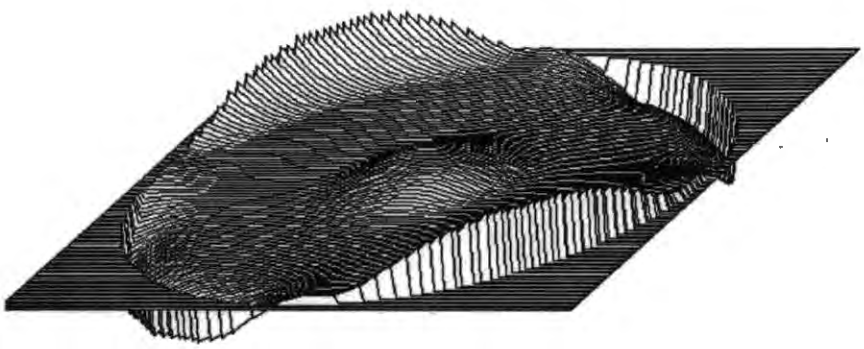

(a)

Figure 2.11.-

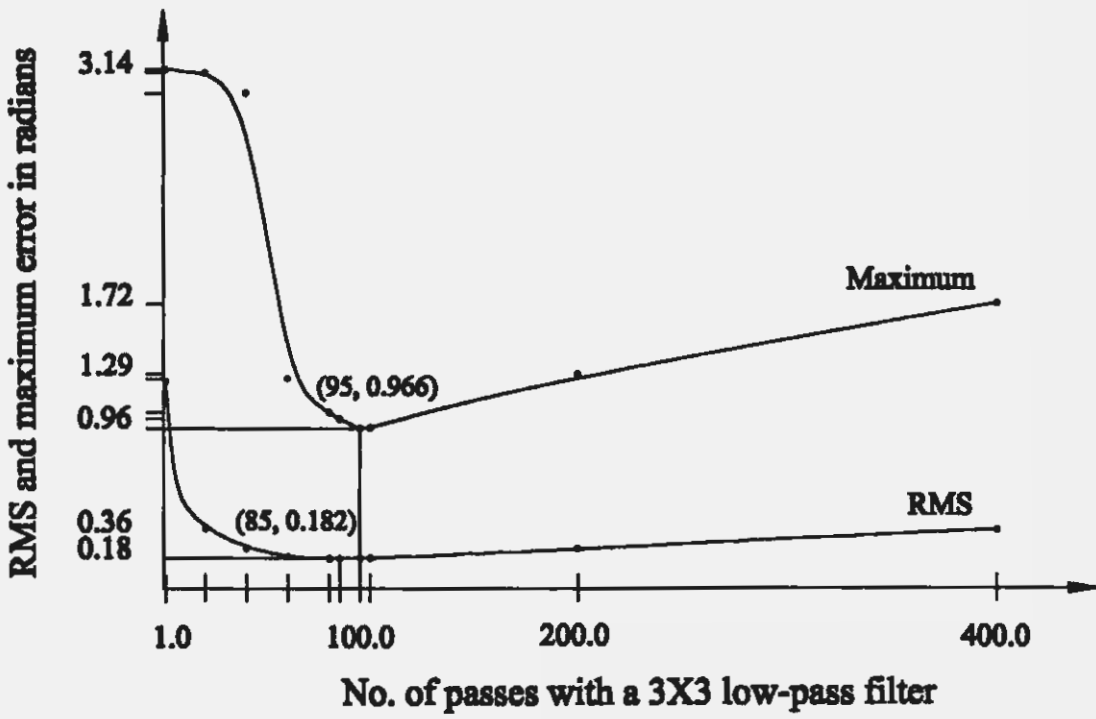
RMS and maximum error in radians
3.14
1.72
1.29
0.96
0.36
0.18
Maximum
RMS
(95, 0.966)
(85, 0.182)
1.0
100.0
200.0
400.0
No. of passes with a 3X3 low-pass filter

Figure 2.12

Chapter III

Holographic and Moiré Aspherical Compensators

3.1 INTRODUCTION

The aim of this chapter is to make an analysis of processes reported as independent in the literature and to establish the relationship between them.

Computer generated aspherical compensators can be superimposed on an aspheric wavefront in an interferometer to produce a null fringe pattern. This process has been widely described in the literature[1,2]. On the other hand, when we superimpose an ideal fringe pattern on top of the picture of an interferogram to be analyzed, we obtain a moiré pattern between the two images. These two apparently different procedures have a lot in common, but also some important and properties that we will describe.

An aspheric wavefront in a Mach-Zehnder, Fizeau or Twyman-Green interferometer produces non-straight fringes with variable fringe spacings as shown in Fig. 3.1(a). If the asphericity is strong, and the tilt is large enough to avoid closed fringes, the minimum fringe spacing may become of the order or smaller than the pixel period in the detector. Then, the sampling theorem limit is exceeded and, the need for an aspheric compensator arises. A computer generated holographic compensator may be used to eliminate the undesired spherical aberration of an aspheric wavefront in order to perform a null test of an aspherical surface, as proposed by several authors, like MacGovern and Wyant[3], Pastor[4], Wyant and Bennett[5] and described in detail by Creath and Wyant[1,2].

The hologram is nothing else but an interferogram made with a large amount of tilt (linear carrier), with a magnitude large enough to separate the diffracted compensated wavefront from the other orders of diffraction, as mentioned by Malacara and Malacara[6]. The wavefront compensation with a hologram can be made in a convergent or a collimated light beam. An example of a computer generated hologram used to eliminate the spherical aberration is shown in Fig. 3.1(b). The tilt in this hologram is almost the same as that in the interferogram in Fig. 3.1(a).

3.2 THEORY

In the holographic compensator the ideal perfect wavefront under test is represented by:

$$W(x, y) = A_W e^{i\phi(x, y)} \tag{3.1}$$

where A_W can be considered a constant and ϕ is the phase of the wavefront under test. This ideal wavefront under test interferes with a flat reference wavefront $R(x, y)$ given by:

$$R(x, y) = A_R e^{i\alpha x} \tag{3.2}$$

where again, A_R is a constant and $\alpha = (2\pi/\lambda)\sin\theta$ andθ is the wavefront Inclination. Thus, the amplitude $E(x, y)$ on the interference plane is

$$E(x, y) = W(x, y) + R(x, y) \tag{3.3}$$

and, the irradiance on the hologram (interferogram) is

$$\begin{aligned} I(x, y) &= E(x, y)\, E^*(x, y) \\ &= A_W^2 + A_R^2 + A_W A_R \left[e^{i(\phi(x, y) - \alpha x)} + e^{-i(\phi(x, y) - \alpha x)} \right] \end{aligned} \tag{3.4}$$

where the symbol * stands for the complex conjugate. If the reconstructing wavefront is $H(x,y)$ given by

$$H(x, y) = A_H e^{i\psi(x, y)} \tag{3.5}$$

Once more A_H is a constant and ψ is the phase of the reconstructing wavefront Assuming a linear recording media, the transmission of the hologram may be considered to be directly proportional to the irradiance in Eq. 4. Thus, upon reconstruction we obtain

$$
\begin{aligned}
G(x, y) = \; & H(x, y)\, I(x, y) \\
& = (A_W^2 + A_R^2)\, A_H\, e^{i\,\psi(x, y)} \\
& + A_W\, A_R\, A_H \left[e^{i\,[\phi(x, y) + \psi(x, y) - \alpha x]} \right] \\
& + A_W\, A_R\, A_H \left[e^{-i\,[(\phi(x, y) - \psi(x, y) - \alpha x]} \right]
\end{aligned}
\tag{3.6}
$$

It must be pointed out that these are the only terms present if we assume a linear recording of the hologram, thus producing sinusoidal fringes. However, a computer generated hologram produces higher order terms not considered here. This is the well known basic hologram theory. Let us now consider three different possible reconstructing schemes.

a) The first case of interest is when the illuminating (reconstructing) wavefront $H(x, y)$ is identical to the flat reference wavefront, given by

$$H(x, y) = R(x, y) \tag{3.7}$$

thus obtaining

$$
\begin{aligned}
G(x, y) = \; & (A_W^2 + A_R^2)\, A_R\, e^{i\,\alpha x} \\
& + A_W\, A_R^2\, e^{i\,\phi(x, y)} + A_W\, A_R^2\, e^{i\,[-\phi(x, y) + 2\,\alpha x]}
\end{aligned}
\tag{3.8}
$$

The first term represents the flat reference wavefront. The second term is the ideal reconstructed wavefront, which is to be compared with the wavefront under test. The third term is a beam conjugate to the first order wavefront reproduced in the -1 order of diffraction. This beam has opposite deformations to those of the first order. Since as pointed out before, the computer generated hologram is not formed by sinusoidal fringes, it has high

order diffracted beams.

b) The second case to consider in Fig. 3.2, is when the illuminating (reconstructing) wavefront $H(x, y)$ is close in shape to the perfect wavefront $W(x, y)$, but with a small difference in phase $\Delta\phi(x, y)$ due to imperfections, as follows

$$\begin{aligned} H(x, y) &= W(x, y)\, e^{i\,\Delta\phi(x, y)} \\ &= A_W\, e^{i\,[\phi(x, y) + \Delta\phi(x, y)]} \end{aligned} \tag{3.9}$$

then, the wavefronts generated by the interferogram are

$$\begin{aligned} G(x, y) = {} & (A_W^2 + A_R^2)\, A_W\, e^{i\,[\phi(x, y) + \Delta\phi(x, y)]} \\ & + A_W^2\, A_R\, e^{i\,[2\,\phi(x, y) + \Delta\phi(x, y) - \alpha x]} \\ & + A_W^2\, A_R\, e^{i\,[\Delta\phi(x, y) + \alpha x]} \end{aligned} \tag{3.10}$$

The first term is the illuminating wavefront. The second term has an asphericity with twice the original magnitude, but with the small deformation of the reconstructing wavefront superimposed. The flat reference wavefront is reproduced only if this wavefront under test is perfect. Otherwise, any deviation from the ideal shape appears on the almost flat wavefront.

c) A third case to consider (Fig.3.3) is when the hologram is illuminated with a wavefront $H(x, y)$ with an asphericity with the opposite sign to the wavefront under test and the small deformation superimposed on it. Thus

$$\begin{aligned} H(x, y) &= W^*(x, y)\, e^{i\,[\,\Delta\phi(x, y) + 2\,\alpha x]} \\ &= A_W\, e^{i\,[-\,\phi(x, y) + \Delta\phi(x, y) + 2\,\alpha x]} \end{aligned} \tag{3.11}$$

where * denotes the complex conjugate, obtaining the following diffracted beams

$$G(x, y) = (A_W^2 + A_R^2) A_W e^{i [- \phi(x, y) + \Delta\phi(x, y) + 2 \alpha x]}$$
$$+ A_W^2 A_R e^{i [\Delta\phi(x, y) + \alpha x]} \qquad (3.12)$$
$$+ A_W^2 A_R e^{i [- 2 \phi(x, y) + \Delta\phi(x, y) + 3 \alpha x]}$$

where the first beam is the illuminating zero order.

The second term is an almost flat wavefront The third term is a wavefront not shown in Fig. 3.4(a). The spectral bandwidths of these beams are directly proportional to the maximum wavefront slope on these wavefronts that, is directly proportional to the maximum interferogram spatial frequency when the tilt is removed. Thus, the bandwidths would increase with their asphericities. Of course, these relative irradiances depend on the fringe profiles.

3.3 HOLOGRAPHIC AND MOIRE COMPENSATORS

The relation between holographic and moiré compensators has been described before[6]. The compensating hologram can be used in three different manners, according to its location in the interferometer. These three manners, which are not the three configuration described in the preceding section, will be described using a Mach-Zehnder interferometer as an example. However, the same principles apply for Fizeau and Twyman-Green interferometers.

3.3.1 Hologram Inside the Interferometer Cavity

The compensating hologram may be placed in the path of the aberrated wavefront,

inside the interferometer cavity, without disturbing the reference wavefront **R**, as in Fig. 3.2(a). Then, the interferogram to be analyzed is formed by the interference between the wavefront under test, after being compensated by the hologram $\mathbf{W}_{+1}$ and the reference wavefront **R**. A total of four wavefronts are produced, the two interfering wavefronts and two extra ones than can be easily low pass filtered, since they travel in different directions and hence different spatial frequencies. This filtering can be performed in the image space by means of common convolution filters using masks or in the Fourier space by means of properly located pinholes.

The spectra of these wavefronts with their relative frequency separations are illustrated in Fig. 3.2(b). The lobe of $\mathbf{W}_0$ should not overlap those of $\mathbf{W}_{+1}$ and **R**. Thus, the minimum linear carrier should be such that the lobes separation is larger than half the width of $\mathbf{W}_0$.

3.3.2 Hologram Outside the Interferometer Cavity

Another possibility is to place the hologram outside the interferometer cavity, in the path of both the wavefront under test and the reference beam, as illustrated in Fig. 3.3(a). Then, both beams will pass through the hologram and reconstruct their own set of wavefronts. The interference now takes place between the zero order (undiffracted) of the reference beam $\mathbf{R}_0$ and the wavefront under test, after being compensated by the hologram $\mathbf{W}_{+1}$. There are six wavefronts, the two interfering wavefronts and four more that should be filtered out. As in the preceding case, the low pass filtering can be performed in the image space as well as in the Fourier space.

The spectra of these wavefronts with their relative frequency separations are illustrated in Fig. 3.3(b). The minimum linear carrier is the same as in the preceding case.

3.3.3 Hologram in front of the Interferogram Picture

Still another possibility is to take a picture of the interferogram with any two wave interferometer, introducing a linear carrier by tilting one of the two wavefronts, and then to

illuminate it with a collimated beam of light as shown in Fig. 3.4(a). Then, the transparency of the interferogram acts a diffracting hologram, generating three wavefronts. One of the interfering wavefronts is the ideal aspheric wavefront produced by the non diffracted beam (zero order) in the interferogram, but diffracted by the compensating hologram. The other interfering wavefront is the wavefront to be measured, produced by diffraction on the interferogram (+1 order) but undiffracted by the compensating hologram (zero order). Besides these two interfering wavefronts, there are seven more, making a total of nine wavefronts. As before, the seven extra undesired wavefronts travel in different directions, thus, with different spatial frequencies. Therefore these wavefronts can also be eliminated by low pass filtering in the image space or in the Fourier space. The Fourier spectrum for this case is in Fig. 3.4(b). The minimum linear carrier is the same as in the other two cases.

These method to compensate with a hologram has traditionally been considered as a moiré process between the actual interferogram and the ideal interferogram. It is however quite interesting to see that it is really a compensating process with a hologram.

3.4 DEMODULATING AN INTERFEROGRAM WITH A LINEAR CARRIER

When analyzing an interferogram to extract the wavefront shape, a phase shifting method is the ideal if an interpolation procedure is to be avoided. Otherwise, if the fringe positions are sampled, the relatively large spacing between the fringes make absolutely necessary a polynomial interpolation, with the well known limitations.

Alternatively, a solution proposed by several researchers to avoid phase shifting, is the introduction of a large linear carrier (a large tilt). Womack[7] proposed a method to demodulate the interferogram in the image space using a method similar to the demodulation procedures used in electronic communications, in order to obtain the phase information (wavefront deformations). On the other hand, Takeda *et al*[8] proposed a method of

demodulation in the Fourier space.

Both demodulations schemes are very powerful, with different advantages and disadventages. A basic requirement is that the linear carrier should be of a magnitude large enough to avoid closed fringes. This condition can be expressed by saying that the minimum linear carrier should be such that the separation between lobes in the Fourier space is larger than half the width of the wide lobe.

The main disadvantage of these methods is the large amount of mathematics and image digitization methods involved. Let us assume that the interferogram linear carrier has to be removed in order to obtain a qualitative assessment of the wavefront. If the wavefront has not been frozen, that is the picture has not been taken, the tilt can very easily be removed in the interferometer by tilting one of the mirrors. However, if the picture is already taken, the only alternative to remove the linear carrier is by moiré with a linear ruling with the same frequency as the linear carrier. This last procedure is basically the same already described here. The only difference is that the compensating hologram is now a linear ruling. Thus, we have nine diffracted wavefronts as in Fig. 3.4(a) with a spectrum for these wavefronts as in Fig. 3.5.

It is interesting to see that the minimum linear carrier to be able to filter the desired wavefronts is when the side lobes just touch the central lobes. It is easy to see now that the minimum linear carrier is that which gives a separation between the lobes equal to the width of the lobes. Thus, the minimum linear carrier in order to use moiré visual demodulation is twice the minimum linear carrier using Womack's or Takeda's demodulation methods. This is an unexpected result.

3.5 REFERENCES

[1] Creath, K. and J. C. Wyant, "Holographic and Speckle Tests", *in Optical Shop Testing*, Chap. 15, D. Malacara, Ed., Second edition, John Wiley & Sons, Inc., New York, (1992a).

[2] Creath, K. and J. C. Wyant, "Moiré and Fringe Projection Techniques", *in Optical Shop Testing*, Chap. 16, D. Malacara, Ed., Second edition, John Wiley & Sons, Inc., New York, (1992b).

[3] MacGovern, A. J., and J. C. Wyant, "Computer Generated Holograms for Testing Optical Elements," *Appl. Opt.*, **10**, 619, (1971).

[4] Pastor J., "Hologram Interferometry and Optical Technology," *Appl. Opt.*, **8**, 525 (1969).

[5] Wyant, J. C. and V. P. Bennett, "Using Computer Generated Hologram to Test Aspheric Wavefronts," *Appl. Opt.*, **11**, 2833 (1972).

[6] Malacara D. and Z. Malacara, "Analogies Between Holographic and Moiré Aspherical Compensators," *Proc. SPIE.*, **2553**, 382 (1995).

[7] Womack K. H., "Interferometric Phase Measurement Using Spatial Synchronous Detection," *Opt. Eng.*, **23**, 391 (1984).

[8] Takeda, M., I. Hideki and S. Kobayashi, "Fourier-Transform Methods of Fringe Pattern Analysis por Computer Based Topography and Interferometry," *J. Opt. Soc. Am.*, **72**, 156 (1982).

[9] García-Márquez, J., D. Malacara-Hernández Z. Malacara and D. Malacara-Doblado, "Holographic and moiré aspherical compensators," *Rev. Mex. Fis.*, accepted, (1998).

Figure Captions

Figure 3.1.- An interferogram of an aspheric wavefront. *a*) with an aberrated aspherical wavefront and *b*) with an ideal aspherical wavefront.

Figure 3.2.- (a) Optical configuration with the hologram inside the interferometer cavity, and (b) spectra of wavefronts.

Figure 3.3.- (a) Optical configuration with hologram outside the interferometer cavity and (b) spectra of wavefronts.

Figure 3.4.- (a) Optical configuration with the hologram in front of the interferogram picture and (b) spectra of wavefronts.

Figure 3.5.- Spectrum when demodulating an interferogram with a linear spatial carrier using moiré with a linear ruling.

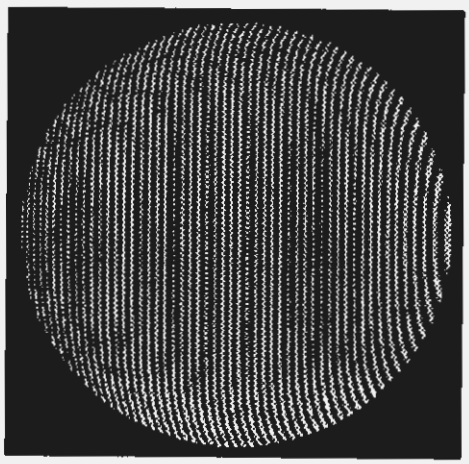

(a)

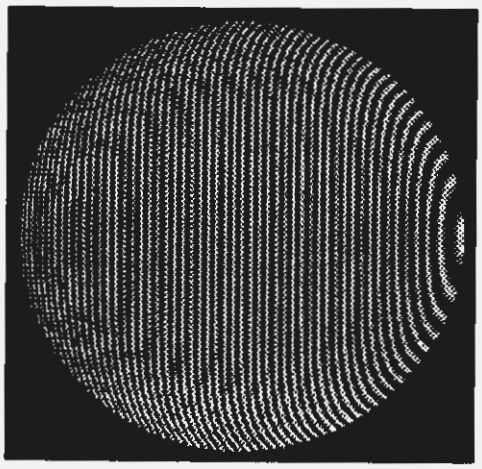

(b)

Figure 3.1.-

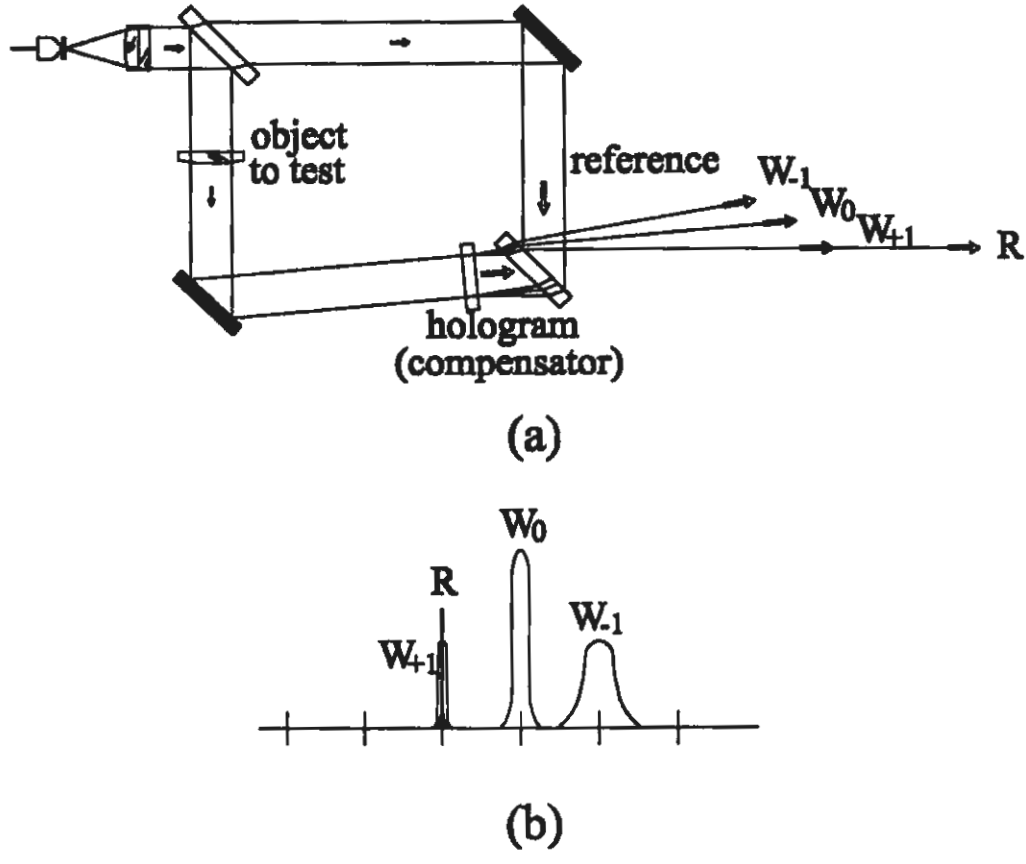
object
to test
reference
W-1
W0
W+1
R
hologram
(compensator)
(a)
W0
R
W-1
W+1
(b)

Figure 3.2.-

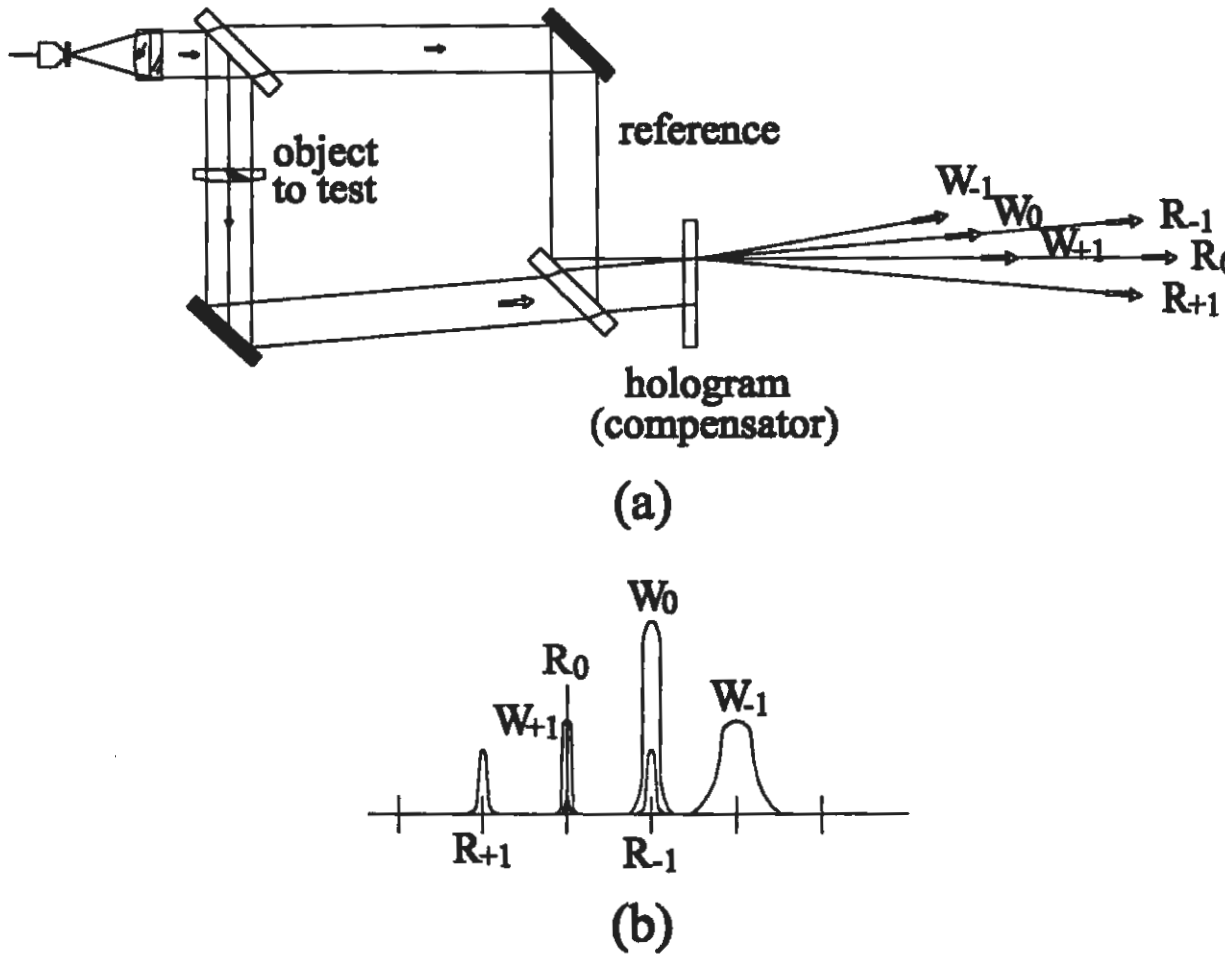
object
to test
reference
W-1
W0
W+1
R-1
R0
R+1
hologram
(compensator)
(a)
W0
R0
W+1
W-1
R+1
R-1
(b)

Figure 3.3.-

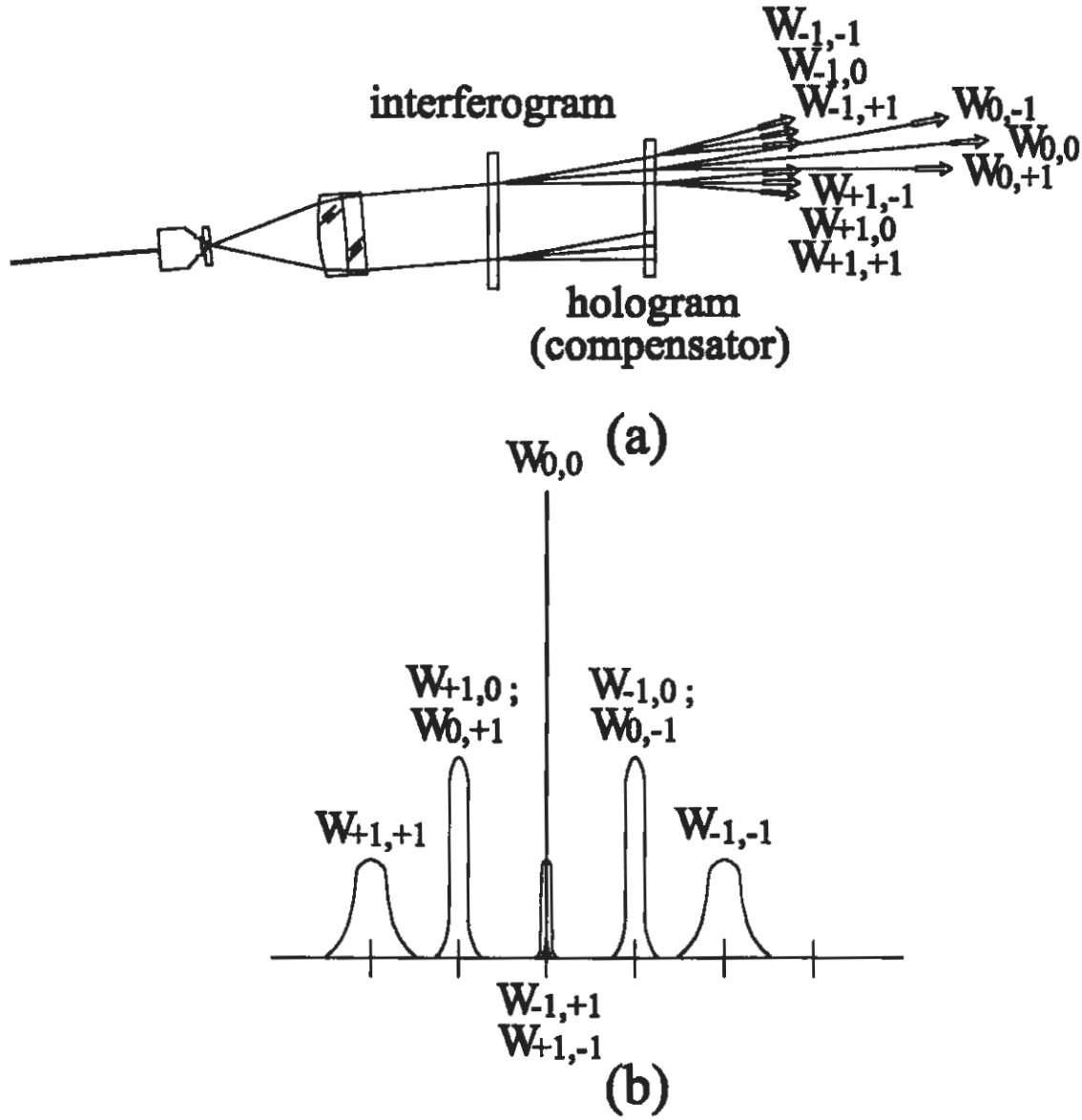
W-1,-1
W-1,0
W-1,+1
W0,-1
W0,0
W0,+1
W+1,-1
W+1,0
W+1,+1
interferogram
hologram
(compensator)
(a)
W0,0
W+1,0 ;
W0,+1
W-1,0 ;
W0,-1
W+1,+1
W-1,-1
W-1,+1
W+1,-1
(b)

Figure 3.4.-

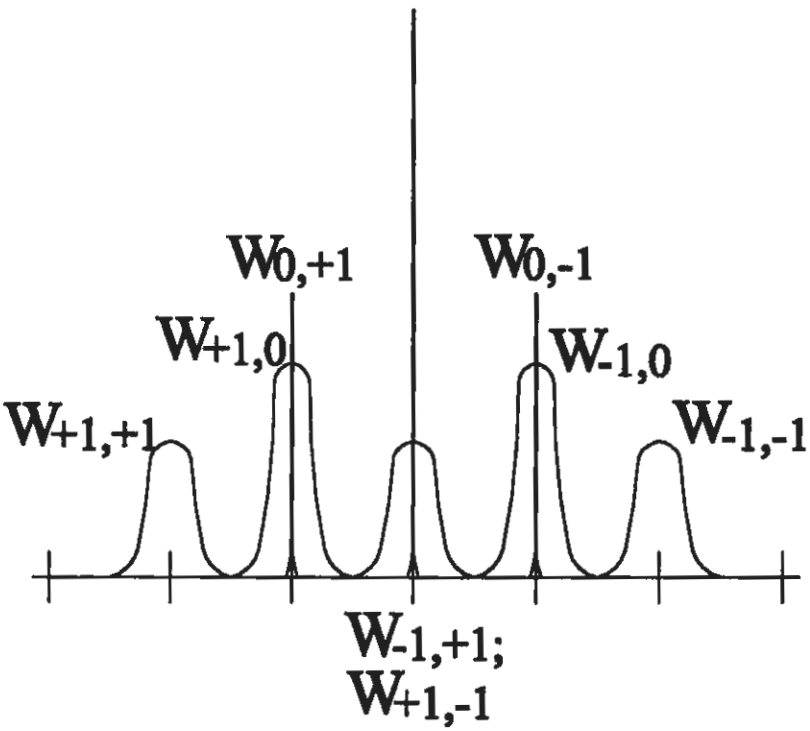

Figure 3.5.-

Conclusions

We have described in this work a fringe analysis methods that enable us to test optical surfaces such as aspheres. In chapter one the different types of fringe analysis when a carrier frequency (linear) is introduced are described with some detail. It is also mentioned the difference between the two main optical methods used in optical metrology the single pattern analysis and the multiple pattern analysis.

It is shown in chapter two that when a radial carrier is encoded in a closed fringe pattern, there, two possible ways to demodulate the interferogram are exposed. These are by means of either an on-axis spherical wavefront or a tilted plane reference respectively. The main advantage of using a spherical or radial carrier is that the closed fringe interferogram may be demodulated without the need of removing the spurious change of the sign of the recovered wavefront. Note that when commercial interferometers test optical surfaces, they need no more than five fringes to have a quite good resolution. More over, Phase Shifting Interferometry requires the existence of low fringes over the field to have a good set of acquisition frames. When using a radial carrier it does not matter whether a large fringe frequency appears in the edges of an interferogram with aspherical aberration. Nevertheless, some problems in the detection of the true phase, due to the incorrect phase information in the center of the interferogram, are present. Despite, when many convolution iterations are made, this error is practically removed. This problem may be attenuated with several passes (85) with a 3x3 convolution filter or fewer passes (29) by means of a 5x5 convolution filter. Besides this another recursive method to reduce the RMS error is proposed. Apart from anything else, the use of a spherical reference limits the kind of closed fringe pattern to those formed by almost concentric closed fringes.

On the other hand the use of a tilted flat reference may be used to demodulate any kind of closed fringe pattern. When the wrong phase in the center of the interferogram appears as in radial demodulation, it is necessary a large time of computational work to solve the reconstruction. In linear carrier demodulation, the time is not the bigger problem, but the appropriate change on the sign in the recovered phase. Besides this, we have discussed the importance of using an appropriate Nx1 convolution mask to low pass-filter, in order to demodulate well.

By the way, interferogram analysis with holographic compensators and with the moiré fringe patterns produced by comparison with a reference grating are essentially the same method, with some differences. It has been shown that, there are three possible ways of measuring an aspheric wavefront using hologram compensators, depending on the position of the holographic compensator. These methods are basically the same method, but have some important practical differences that can decide which method is best in a given case.

The theoretical and conceptual differences between demodulating an interferogram with a linear carrier using digitalization and mathematical procedures and the analog moiré demodulation method had been pointed out. Of course, if the reconstruction of a closed wavefront should be made by using a radial reference wavefront, conditions on the Fourier plane changes.

Conclusiones

Durante el tiempo que duró esta investigación, hemos encontrado un método que nos permite probar superficies ópticas asféricas. En el introductorio capítulo uno, se mencionan con detalle los diferentes métodos de análisis de franjas con introducción de portadora lineal. También hacemos mención de las diferencias entre los dos principales métodos ópticos usados en metrología óptica; el análisis de patrones sencillos y el análisis de patrones múltiples.

En el capítulo dos demostramos que si se utiliza una portadora radial codificada en un patrón de franjas cerradas, podremos extraer la fase por cualesquiera de dos métodos propuestos. En uno utilizamos un frente de onda esférico en eje (muy similar a aquel codificado en el interferograma) mientras que en el otro se hace por medio de un frente de onda de referencia plano e inclinado. En el primer caso, encontramos algunas ventajas importantes. Primero, se recupera la fase del patrón de franjas cerradas sin la necesidad de remover el cambio de signo parásito, como se acontece en los métodos propuestos por Kreis y Moore. La siguiente ventaja es que no importa que en el borde halla una alta frecuencia espacial, ésto conlleva a que si el interferograma tiene una fuerte concentración de franjas puede ser demodulado. No pasa así en los interferómetros comerciales, donde el interferograma obtenido por dos superficies, la de referencia y la de prueba, debe tener no más de cinco franjas. Mas aún, la Interferometría de Desplazamiento de Fase tradicional requiere la existencia de relativamente pocas franjas. Considere que el dispositivo de desplazamiento necesita ser operado con un margen de movimiento bastante mayor que el límite de Nyquist (entre 10 y 20 franjas a lo mucho). Sin embargo, el método presenta algunos inconvenientes. La falta de información (carencia de franjas) en el centro del

interferograma provoca una detección erronea de la fase. Este problema se puede resolver por un multiple paso (85) de un filtro de convolución de 3x3 o bién menos pasos (29) con un filtro de 5x5. Se propone como alternativa un método recursivo para minimizar tanto el número de pasos (mucho tiempo de trabajo computacional), como el error cuadrático medio. Otro de los inconvenientes es que el uso de la referencia esférica limita la prueba a patrones de franjas cerradas pseudoconcéntricas.

Por otro lado, podemos hacer uso de una referencia plana e inclinada para demodular cualquier tipo de patrones de franjas cerradas. El inconveniente de este método, deja de ser la falta de información en el centro del patrón de franjas, el verdadero problema tiene su origen en el método mismo. Es decir, al igual que los métodos propuestos por Kreis y por Moore, la ambiguedad en el signo de la fase recuperada se hace presente. Por otro lado, debemos hacer resaltar que se debe utilizar una máscarilla de convolución rectangular Nx1 para realizar el filtraje pasa bajas y demodular en forma conveniente.

Finalmente, el capítulo tres se enfoca en el análisis de interferogramas con compensadores holográficos y con patrones de franjas de moiré, producidos por comparación con una rejilla de referencia. Tradicionalmente se ha pensado que es el mismo método, la realidad es que tiene algunas diferencias. Se ha mostrado que, existen tres posibles formas de medir un frente de onda asférico por medio de compensadores holográficos, dependiendo de la posición misma del compensador. Aunque los métodos de prueba son básicamente iguales, tienen algunas diferencias prácticas importantes que, dependiendo del caso, pueden hacernos decidir por el más conveniente.

Por último, se han señalado las diferencias entre demodular un interferograma con una portadora lineal, por medio de una digitalización y un trabajo matemático y el análogo método de moiré. Por supuesto, las condiciones cambian si se elijen las técnicas de portadora circular.

List of Publications by the Author

Refered Papers

[1] Malacara-Doblado, D., D. Malacar- Hernández and J. García-Márquez, "Axially astigmatic surfaces: different types and their properties," *Opt. Eng.*, **35**(12), 3422-3426 (1996).

[2] García-Márquez, J., D. Malacara-Hernández and D. Malacara-Doblado., "Interferometers without observable fringes," *Opt. Eng.* **36**(10), 2863-2867 (1997).

[3] García-Márquez, J., D. Malacara-Hernández and M. Servín, "Analysis of interferograms with a spatial radial carrier or closed fringes, and its holographic analogy," *Appl. Opt.* **37**(34), (1998).

[4] García-Márquez, J., D. Malacara-Hernández, and Z. Malacara, "Holographic and moiré aspherical compensators," *Rev. Méx. Fís.*, No. de Reg. 1871.

Conference Papers

[1] García-Márquez, J., D. Malacara-Hernández and D. Malacara-Doblado, "Interferometers Without Fringe Patterns," *Proc. SPIE*, **2576**, 323 (1995).

[2] García-Márquez, J. and D. Malacara-Hernández, "Holographic Analogy of the Spatial Radial Carrier Analysis of Interferograms," *Proc. SPIE*, **2860**, 394 (1996).